

# 1 **Historical and future contributions of inland waters to the Congo basin**

## 2 **carbon balance**

3 Adam Hastie<sup>1,2</sup>, Ronny Lauerwald<sup>2,3,4</sup>, Philippe Ciais<sup>3</sup>, Fabrice Papa<sup>5,6</sup>, Pierre Regnier<sup>2</sup>

4

5 <sup>1</sup>School of GeoSciences, University of Edinburgh, EH9 3FF, Edinburgh, Scotland, UK

6 <sup>2</sup>Biogeochemistry and Earth System Modelling, Department of Geoscience, Environment and  
7 Society, Université Libre de Bruxelles, Bruxelles, 1050, Belgium

8 <sup>3</sup>Laboratoire des Sciences du Climat et de l'Environnement (LSCE), CEA CNRS UVSQ, Gif-  
9 sur-Yvette 91191, France

10 <sup>4</sup>Université Paris-Saclay, INRAE, AgroParisTech, UMR ECOSYS, 78850, Thiverval-Grignon,  
11 France

12 <sup>5</sup>Laboratoire d'Etudes en Géophysique et Océanographie Spatiales, Centre National de la  
13 Recherche Scientifique–Institut de recherche pour le développement–Université Toulouse Paul  
14 Sabatier–Centre national d'études spatiales, 31400 Toulouse, France

15 <sup>6</sup>UnB, Universidade de Brasília, Institute of Geosciences, Campus Universitario Darcy Ribeiro,  
16 70910-900 Brasilia (DF), Brazil

17 *Correspondence to:* Adam Hastie (adam.hastie@ed.ac.uk)

18

## 19 **Abstract**

20 As the second largest area of contiguous tropical rainforest and second largest river basin in  
21 the world, the Congo basin has a significant role to play in the global carbon (C) cycle. For the  
22 present day, it has been shown that a significant proportion of global terrestrial net primary  
23 productivity (NPP) is transferred laterally to the land-ocean aquatic continuum (LOAC) as  
24 dissolved CO<sub>2</sub>, dissolved organic carbon (DOC) and particulate organic carbon (POC). Whilst  
25 the importance of LOAC fluxes in the Congo basin has been demonstrated for the present day,  
26 it is not known to what extent these fluxes have been perturbed historically, how they are likely  
27 to change under future climate change and land use scenarios, and in turn what impact these  
28 changes might have on the overall C cycle of the basin. Here we apply the ORCHILEAK model  
29 to the Congo basin and estimate that 4% of terrestrial NPP (NPP = 5,800 ±166 Tg C yr<sup>-1</sup>) is  
30 currently exported from soils and vegetation to inland waters. Further, our results suggest that

31 aquatic C fluxes may have undergone considerable perturbation since 1861 to the present day,  
32 with aquatic CO<sub>2</sub> evasion and C export to the coast increasing by 26% (186 ±41 Tg C yr<sup>-1</sup> to  
33 235 ±54 Tg C yr<sup>-1</sup>) and 25% (12 ±3 Tg C yr<sup>-1</sup> to 15 ±4 Tg C yr<sup>-1</sup>) respectively, largely because  
34 of rising atmospheric CO<sub>2</sub> concentrations. Moreover, under climate scenario RCP 6.0 we  
35 predict that this perturbation could continue; over the full simulation period (1861-2099), we  
36 estimate that aquatic CO<sub>2</sub> evasion and C export to the coast could increase by 79% and 67%  
37 respectively. Finally, we show that the proportion of terrestrial NPP lost to the LOAC could  
38 increase from approximately 3% to 5% from 1861-2099 as a result of increasing atmospheric  
39 CO<sub>2</sub> concentrations and climate change. However, our future projections of the Congo basin C  
40 fluxes in particular need to be interpreted with some caution due to model limitations. We  
41 discuss these limitations, including the wider challenges associated with applying the current  
42 generation of land surface models which ignore nutrient dynamics to make future projections  
43 of the tropical C cycle, along with potential next steps.

## 44 **1. Introduction**

45 As the world's second largest area of contiguous tropical rainforest and second largest river,  
46 the Congo basin has a significant role to play in the global carbon (C) cycle. Current estimates  
47 of its C stocks and fluxes are limited by a paucity of field data and therefore have substantial  
48 uncertainties, both quantified and unquantified (Williams et al., 2007; Lewis et al., 2009;  
49 Dargie et al., 2017). Nevertheless, it has been estimated that there is approximately 50 Pg C  
50 stored in its above ground biomass (Verhegghen et al., 2012), and up to 100 Pg C contained  
51 within its soils (Williams et al., 2007). Moreover, a recent study estimated that around 30 (6.3–  
52 46.8) Pg C is stored in the peats of the Congo alone (Dargie et al., 2017). Field data suggest  
53 that storage in tree biomass increased by 0.34 (0.15- 0.43) Pg C yr<sup>-1</sup> in intact African tropical  
54 forests between 1968-2007 (Lewis et al., 2009) due in large part to a combination of increasing  
55 atmospheric CO<sub>2</sub> concentrations and climate change (Ciais et al., 2009; Pan et al., 2015), while

56 satellite data indicates that terrestrial net primary productivity (NPP) has increased by an  
57 average of  $10 \text{ g C m}^{-2} \text{ yr}^{-1}$  per year between 2001 and 2013 in tropical Africa (Yin et al., 2017).

58 At the same time, forest degradation, clearing for rotational agriculture and logging are causing  
59 C losses to the atmosphere (Zhuravleva et al., 2013; Tyukavina et al., 2018) while droughts  
60 have reduced vegetation greenness and water storage over the last decade (Zhou et al., 2014).

61 A recent estimate of above ground C stocks of tropical African forests, mainly in the Congo,  
62 indicates a minor net C loss from 2010 to 2017 (Fan et al., 2019). Moreover, recent field data  
63 suggests that the above ground C sink in tropical Africa was relatively stable from 1985 to  
64 2015 (Hubau et al., 2020).

65 There are large uncertainties associated with projecting future trends in the Congo basin  
66 terrestrial C cycle, firstly related to predicting which trajectories of future  $\text{CO}_2$  levels and land  
67 use changes will occur, and secondly to our ability to fully understand and simulate these  
68 changes and in turn their impacts. Future model projections for the 21<sup>st</sup> century agree that  
69 temperature will significantly increase under both low and high emission scenarios (Haensler  
70 et al., 2013), while precipitation is only projected to substantially increase under high emission  
71 scenarios, the basin mean remaining more or less unchanged under low emission scenarios  
72 (Haensler et al., 2013). Uncertainties in future land-use change projections for Africa are  
73 among the highest for any continent (Hurtt et al., 2011).

74 For the present day at the global scale, it has been estimated that between 1 and  $5 \text{ Pg C yr}^{-1}$  is  
75 transferred laterally to the land-ocean aquatic continuum (LOAC) as dissolved  $\text{CO}_2$ , dissolved  
76 organic carbon (DOC) and particulate organic carbon (POC) (Cole et al., 2007; Tranvik et al.,  
77 2009; Regnier et al., 2013; Drake et al., 2018; Ciais et al. 2020). This C can subsequently be  
78 evaded back to the atmosphere as  $\text{CO}_2$ , undergo sedimentation in wetlands and inland waters,  
79 or be transported to estuaries or the coast. The tropical region is a hotspot area for inland water

80 C cycling (Richey et al., 2002; Melack et al., 2004; Abril et al., 2014; Borges et al., 2015<sup>a</sup>;  
81 Lauerwald et al., 2015) due to high terrestrial NPP and precipitation, and a recent study used  
82 an upscaling approach based on observations to estimate present day CO<sub>2</sub> evasion from the  
83 rivers of the Congo basin at 251±46 Tg C yr<sup>-1</sup> and the lateral C (TOC +DIC) export to the coast  
84 at 15.5 (13-18) Tg C yr<sup>-1</sup> (Borges et al., 2015<sup>a</sup>; Borges et al., 2019). To put this into context,  
85 their estimate of aquatic CO<sub>2</sub> evasion represents 39% of the global value estimated by  
86 Lauerwald et al. (2015, 650 Tg C yr<sup>-1</sup>) or 14% of the global estimate of Raymond et al. (2013,  
87 1,800 Tg C yr<sup>-1</sup>). Note that while Lauerwald et al. (2015) and Raymond et al. (2013) relied  
88 largely on the same database of partial pressure of CO<sub>2</sub> (*p*CO<sub>2</sub>) measurements (GloRiCh,  
89 Hartmann et al., 2014) as the basis for their estimates, they took different, albeit both  
90 empirically led approaches. Moreover, both approaches were limited by a relative paucity of  
91 data from the tropics, which also explains the high degree of uncertainty associated with our  
92 understanding of global riverine CO<sub>2</sub> evasion.

93 Whilst the importance of LOAC fluxes in the Congo basin has been demonstrated for the  
94 present day, it is not known to what extent these fluxes have been perturbed historically, how  
95 they are likely to change under future climate change and land use scenarios, and in turn what  
96 impact these changes might have on the overall C balance of the Congo. In light of these  
97 knowledge gaps, we address the following research questions:

- 98 • What is the relative contribution of LOAC fluxes (CO<sub>2</sub> evasion and C export to the  
99 coast) to the present-day C balance of the basin?
- 100 • To what extent have LOAC fluxes changed from 1860 to the present day and what are  
101 the primary drivers of this change?
- 102 • How will these fluxes change under future climate and land use change scenarios (RCP  
103 6.0 which represents the “no mitigation scenario”) and what are the limitations  
104 associated with these future projections?

105

106 Understanding and quantifying these long-term changes requires a complex and integrated  
107 mass-conservation modelling approach. The ORCHILEAK model (Lauerwald et al., 2017), a  
108 new version of the land surface model ORCHIDEE (Krinner et al., 2005), is capable of  
109 simulating observed terrestrial and aquatic C fluxes in a consistent manner for the present day  
110 in the Amazon (Lauerwald et al., 2017) and Lena (Bowring et al., 2019<sup>a</sup>; Bowring et al., 2019<sup>b</sup>)  
111 basins, albeit with limitations including a lack of explicit representation of POC fluxes and in-  
112 stream autotrophic production (see Lauerwald et al., 2017; Bowring et al., 2019<sup>a</sup>; Bowring et  
113 al., 2019<sup>b</sup> and Hastie et al., 2019 for further discussion). Moreover, it was recently demonstrated  
114 that this model could recreate observed seasonal and interannual variation in Amazon aquatic  
115 and terrestrial C fluxes (Hastie et al., 2019).

116 In order to accurately simulate aquatic C fluxes, it is crucial to provide a realistic representation  
117 of the hydrological dynamics of the Congo River, including its wetlands. Here, we develop  
118 new wetland forcing files for the ORCHILEAK model from the high-resolution dataset of  
119 Gumbrecht et al. (2017) and apply the model to the Congo basin. After validating the model  
120 against observations of discharge, flooded area, DOC concentrations and  $p\text{CO}_2$  for the present  
121 day, we then use the model to understand and quantify the long- term (1861-2099) temporal  
122 trends in both the terrestrial and aquatic C fluxes of the Congo Basin.

## 123 **2. Methods**

124 ORCHILEAK (Lauerwald et al., 2017) is a branch of the ORCHIDEE land surface model  
125 (LSM), building on past model developments such as ORCHIDEE-SOM (Camino Serrano,  
126 2018), and represents one of the first LSM-based approaches which fully integrates the aquatic  
127 C cycle within the terrestrial domain. ORCHILEAK simulates DOC production in the canopy  
128 and soils, the leaching of dissolved  $\text{CO}_2$  and DOC to the river from the soil, the mineralization  
129 of DOC, and in turn the evasion of  $\text{CO}_2$  to the atmosphere from the water surface. Moreover,

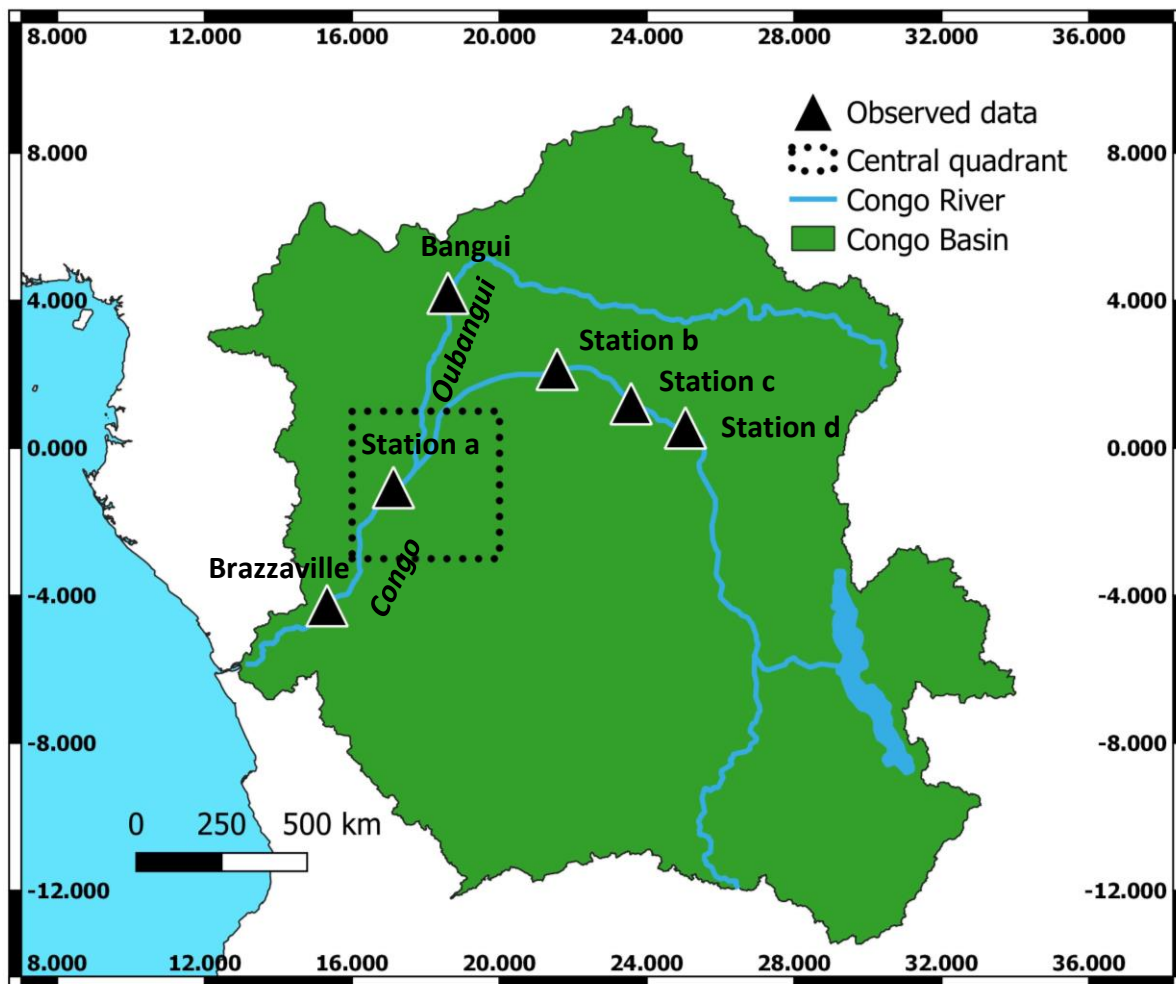
130 it represents the transfer of C between litter, soils and water within floodplains and swamps  
131 (see section 2.2). Once within the river routing scheme, ORCHILEAK assumes that the lateral  
132 transfer of CO<sub>2</sub> and DOC are proportional to the volume of water. DOC is divided into a  
133 refractory and labile pool within the river, with half-lives of 80 and 2 days respectively. The  
134 refractory pool corresponds to the combined slow and passive DOC pools of the soil C scheme,  
135 and the labile pool corresponds to the active soil pool (see section 2.4.1). The concentration of  
136 dissolved CO<sub>2</sub> and the temperature-dependent solubility of CO<sub>2</sub> are used to calculate *p*CO<sub>2</sub> in  
137 the water column. In turn, CO<sub>2</sub> evasion is calculated based on *p*CO<sub>2</sub>, along with a diurnally  
138 variable water surface area and a gas exchange velocity. Fixed gas exchange velocities of 3.5  
139 m d<sup>-1</sup> and 0.65 m d<sup>-1</sup> respectively are used for rivers (including open floodplains) and forested  
140 floodplains.

141 In this study, as in previous studies (Lauerwald et al., 2017, Hastie et al. 2019, Bowring et al.,  
142 2019<sup>a,b</sup>), we run the model at a spatial resolution of 1° and use the default time step of 30 min  
143 for all vertical transfers of water, energy and C between vegetation, soil and the atmosphere,  
144 and the daily time-step for the lateral routing of water. Until now, in the Tropics, ORCHILEAK  
145 has been parameterized and calibrated only for the Amazon River basin (Lauerwald et al., 2017,  
146 Hastie et al. 2019). To adapt and apply ORCHILEAK to the specific characteristics of the  
147 Congo River basin (2.1), we had to establish new forcing files representing the maximal  
148 fraction of floodplains (MFF) and the maximal fraction of swamps (MFS) (2.2) and to  
149 recalibrate the river routing module of ORCHILEAK (2.3). All of the processes represented in  
150 ORCHILEAK remain identical to those previously represented for the Amazon ORCHILEAK  
151 (Lauerwald et al., 2017; Hastie et al., 2019). In the following methodology sections, we  
152 describe; 2.1- Congo basin description, 2.2- Development of floodplains and swamps forcing  
153 files, 2.3- Calibration of hydrology, 2.4- Simulation set-up, 2.5- Evaluation and analysis of

154 simulated fluvial C fluxes, and 2.6- Calculating the net carbon balance of the Congo Basin. For  
155 a full description of the ORCHILEAK model please see Lauerwald et al. (2017).

## 156 2.1 Congo basin description

157 The Congo Basin is the world's second largest area of contiguous tropical rainforest and second  
158 largest river basin in the world (Fig. 1), covering an area of  $3.7 \times 10^6 \text{ km}^2$ , with a mean discharge  
159 of around  $42,000 \text{ m}^3 \text{ s}^{-1}$  (O'Loughlin et al., 2013) and a variation between  $24,700\text{--}75,500 \text{ m}^3$   
160  $\text{s}^{-1}$  across months (Coynel et al., 2005).

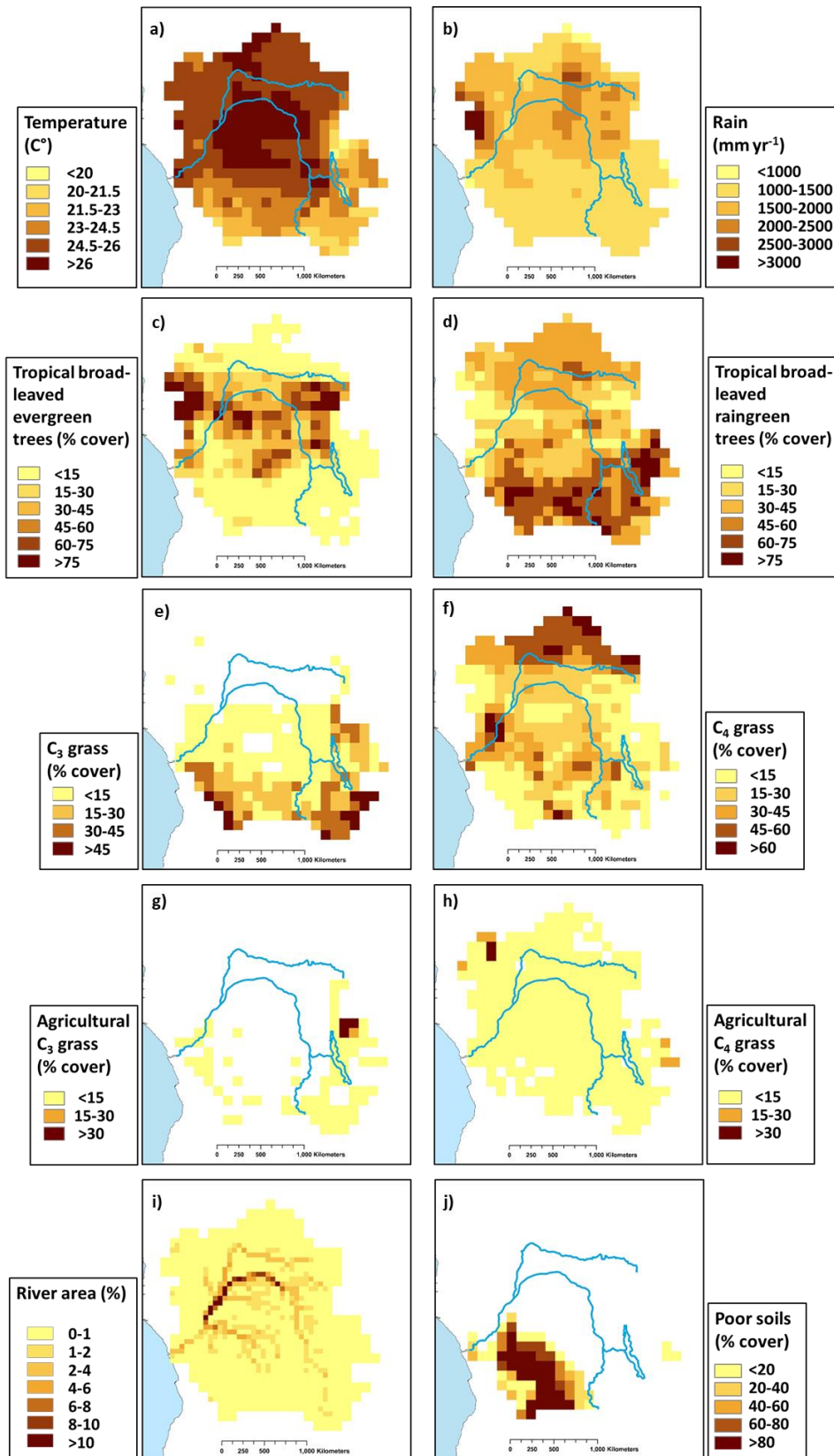


161  
162 **Figure 1:**Extent of the Congo Basin, central quadrant of the “Cuvette Centrale” and sampling  
163 stations (for DOC and discharge) along the Congo and Oubangui Rivers (in italic).

164

165 The major climate (ISMSIP2b, Frieler et al., 2017; Lang et al., 2017) and land-cover (LUH-  
166 CMIP5) characteristics of the Congo Basin for the present day (1981-2010) are shown in Figure  
167 2. The mean annual temperature is 25.2 °C but with considerable spatial variation from a low  
168 of 18.4°C to a high of 27.2°C (Fig. 2 a), while mean annual rainfall is 1520mm, varying from  
169 733 mm to 4087 mm (Fig. 2 b). ORCHILEAK prescribes 13 different plant functional types  
170 (PFTs). Land-use is mixed with tropical broad-leaved evergreen (PFT2, Fig. 1 c), tropical  
171 broad-leaved rain green (PFT3, Fig. 1 d), C<sub>3</sub> grass (PFT10, Fig. 2 e) and C<sub>4</sub> grass (PFT11, Fig.  
172 2 f) covering a maximum of 26%, 35%, 8% and 25% of the basin area respectively (Table A3).  
173 Most published estimates for land-cover follow national boundaries and so we can make broad  
174 comparisons with published estimates for the Democratic Republic of Congo (DRC). For  
175 example, our value for total forest cover for the DRC (65%), is close to the 67% and 68%  
176 values estimated by the Congo Basin Forest Partnership (CBFP, 2009), and Potapov et al.  
177 (2012), respectively. Agriculture covers only a small proportion of the basin according to the  
178 LUH dataset that is based on FAO cropland area statistics, with C<sub>3</sub> (PFT12, Fig. 2 g) and C<sub>4</sub>  
179 (PFT13, Fig. 2 h) agriculture making up a maximum basin area of 0.5 and 2% respectively. In  
180 reality, a larger fraction of the basin is composed of small scale and rotational agriculture  
181 (Tyukavina et al., 2018). The ORCHILEAK model also has a “poor soils” forcing file (Fig. 2  
182 j) which prescribes reduced decomposition rates in soils with low nutrient and pH soils such as  
183 Podzols and Arenosols (Lauerwald et al., 2017). This file is developed from the Harmonized  
184 World Soil Database (FAO/IIASA/ISRIC/ISS-CAS/JRC, 2009).





185

186 **Figure 2: Present day (1981-2010) spatial distribution of the principal climate and land-use**  
 187 **drivers used in ORCHILEAK, across the Congo Basin; a) mean annual temperature in °C, b)**  
 188 **mean annual rainfall in mm yr<sup>-1</sup>, c)-h) mean annual maximum vegetated fraction for PFTs 2,3,**

189 **10,11,12 and 13, i) river area, and j) Poor soils. All at a resolution of 1° except for river area**  
190 **(0.5°).**

## 191 **2.2 Development of floodplains and swamps forcing files**

192 In ORCHILEAK, water in the river network can be diverted to two types of wetlands,  
193 floodplains and swamps. In each grid where a floodplain exists, a temporary waterbody can be  
194 formed adjacent to the river and is fed by the river once bank-full discharge (see section 2.3)  
195 is exceeded. In grids where swamps exist, a constant proportion of river discharge is fed into  
196 the base of the soil column; ORCHILEAK does not explicitly represent a groundwater reservoir  
197 and so this imitates the hydrological coupling of swamps and rivers through the groundwater  
198 table. The maximal proportions of each grid which can be covered by floodplains and swamps  
199 are prescribed by the maximal fraction of floodplains (MFF) and the maximal fraction of  
200 swamps (MFS) forcing files respectively (Guimberteau et al., 2012). See also Lauerwald et al.  
201 (2017) and Hastie et al. (2019) for further details. We created an MFF forcing file for the Congo  
202 basin, derived from the Global Wetlands<sup>v3</sup> database; the 232 m resolution tropical wetland map  
203 of Gumbricht et al. (2017) (Fig. 3 a and b). We firstly amalgamated all the categories of wetland  
204 (which include floodplains and swamps) before aggregating them to a resolution of 0.5° (the  
205 resolution at which the floodplain/swamp forcing files are read by ORCHILEAK), assuming  
206 that this represents the maximum extent of inundation in the basin. This results in a mean MFF  
207 of 10%, i.e. a maximum of 10% of the surface area of the Congo basin can be inundated with  
208 water. This is identical to the mean MFF value of 10% produced with the Global Lakes and  
209 Wetlands Database, GLWD (Lehner, & Döll, P.,2004; Borges et al., 2015<sup>b</sup>). We also created  
210 an MFS forcing file from the same dataset (Fig. 3 c and d), merging the ‘swamps’ and ‘fens’  
211 wetland categories (although note that there are virtually no fens in the Congo basin) from  
212 Global Wetlands<sup>v3</sup> database (Gumbricht et al., 2017) and again aggregating them to a 0.5°  
213 resolution. Please see Table 1 of Gumbricht et al. (2017) for further details.

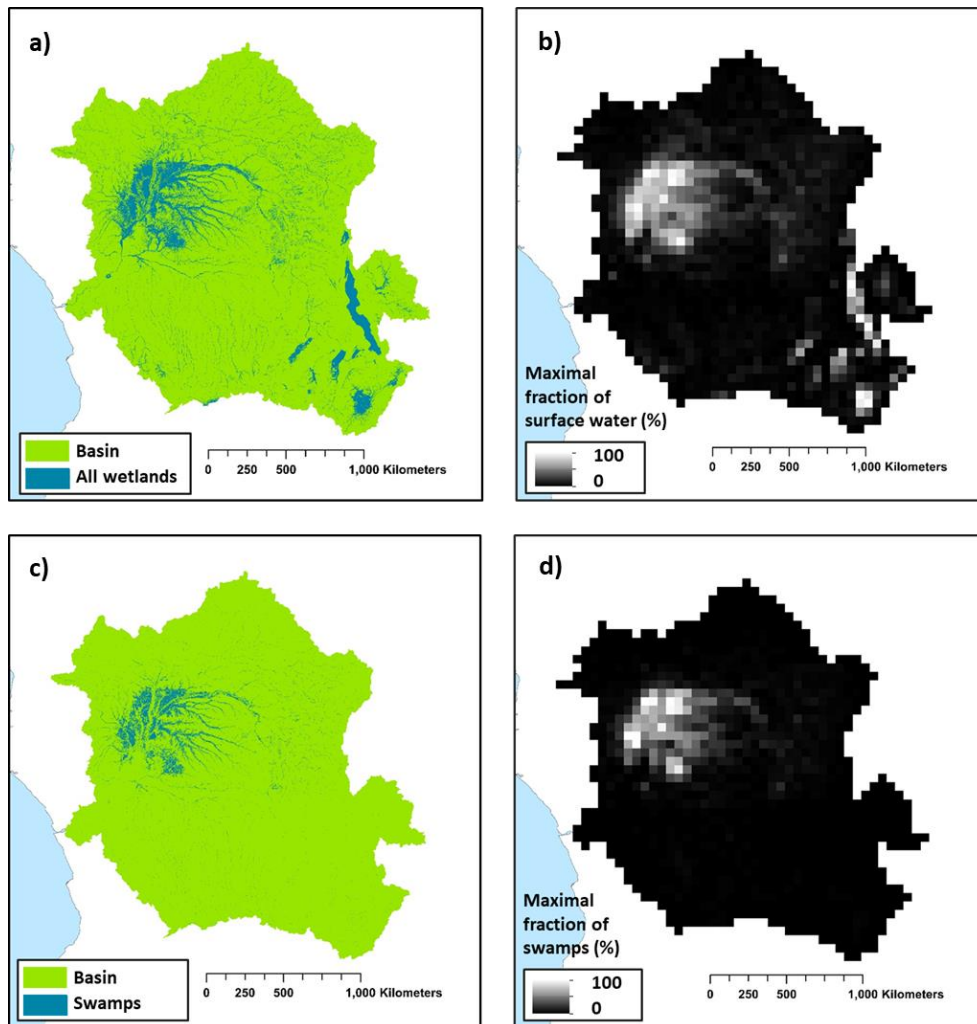


Figure 3: a) Wetland extent (from Gumbricht et al., 2017). b) The new maximal fraction of floodplain (MFF) forcing file developed from a). c) Swamps (including fens) category within Congo basin from Gumbricht et al (2017). d) the new maximal fraction of swamps (MFS) forcing file developed from c). Panels a) and b) are at the same resolution as the Gumbricht dataset (232m) while b) and d) are at a resolution of 0.5°. Note that 0.5° is the resolution of the sub unit basins in ORCHILEAK (Lauerwald et al., 2015), with each 1° grid containing four sub basins.

214

### 215 2.3 Calibration of hydrology

216 As the main driver of the export of C from the terrestrial to aquatic system, it is crucial that the  
 217 model can represent present-day hydrological dynamics, at the very least on the main stem of  
 218 the Congo. As this study is primarily concerned with decadal- centennial timescales our priority  
 219 was to ensure that the model can accurately recreate observed mean annual discharge at the  
 220 most downstream gauging station Brazzaville. We also tested the model's ability to simulate

221 observed discharge seasonality, as well as flood dynamics. Moreover, no data is available with  
222 which to directly evaluate the simulation of DOC and CO<sub>2</sub> leaching from the soil to the river  
223 network, and thus we tested the model's ability to recreate the spatial variation of observed  
224 riverine DOC concentrations and *p*CO<sub>2</sub> at specific stations where measurements are available  
225 (Borges et al., 2015<sup>b</sup>; Bouillon et al., 2012 & 2014, locations shown in Fig. 1), river DOC and  
226 CO<sub>2</sub> concentration being regarded as an integrator of the C transport at the terrestrial-aquatic  
227 interface.

228 We first ran the model for the present-day period, defined as from 1990 to 2005/2010  
229 depending on which climate forcing data was applied, using four climate forcing datasets;  
230 namely ISIMIP2b (Frieler et al., 2017), Princeton GPCP (Sheffield et al., 2006), GSWP3 (Kim,  
231 2017) and CRUNCEP (Viovy, 2018). We used ISIMIP2b for the historical and future  
232 simulations as it is the only climate forcing dataset to cover the full period (1861-2099).  
233 However, we compared it to other climate forcing datasets for the present day in order to gauge  
234 its ability to simulate observed discharge on the Congo River at Brazzaville (Table A1).  
235 Without calibration, the majority of the different climate forcing model runs performed poorly,  
236 unable to accurately represent the seasonality and mean monthly discharge at Brazzaville  
237 (Table A1). The best performing climate forcing dataset was ISIMIP2b followed by Princeton  
238 GPCP with root mean square errors (RMSE) of 29% and 40% and Nash Sutcliffe efficiencies  
239 (NSE) of 0.20 and -0.25, respectively. NSE is a statistical coefficient specifically used to test  
240 the predictive skill of hydrological models (Nash & Sutcliffe, 1970).

241 For ISIMIP2b we further calibrated key hydrological model parameters, namely the constants  
242 ( $\tau$ ,  $\tau$ ) which help to control the water residence time of the groundwater (=slow reservoir),  
243 headwaters (= fast reservoir) and floodplain reservoirs in order to improve the simulation of  
244 observed discharge at Brazzaville and Oubangui (Table 2). To do so, we tested different  
245 combinations of  $\tau$  values for the three reservoirs, eventually settling on 1, 0.5 and 0.5 (days)

246 for the slow, fast and floodplain reservoirs respectively, all three being reduced compared to  
247 those values used in the original ORCHILEAK calibration for the Amazon (Lauerwald et al.,  
248 2017). The actual residence time of each reservoir is calculated at each time step. The residence  
249 time of the flooded reservoir for example, is a product of  $\tau_{\text{flood}}$ , a topographical index and the  
250 flooded fraction of the grid cell.

251 In order to calibrate the simulated discharge against observations, we first modified the flood  
252 dynamics of ORCHILEAK in the Congo Basin for the present day by adjusting bank-full  
253 discharge ( $\text{streamr}_{50\text{th}}$ , Lauerwald et al., 2017) and 95<sup>th</sup> percentile of water level heights  
254 ( $\text{floodh}_{95\text{th}}$ ). As in previous studies on the Amazon basin (Lauerwald et al. 2017, Hastie et al.,  
255 2019) we defined bank-full discharge, i.e. the threshold discharge at which floodplain  
256 inundation starts (i.e. overtopping of banks), as the median discharge (50<sup>th</sup> percentile i.e.  
257  $\text{streamr}_{50\text{th}}$ ) of the present-day climate forcing period (1990 to 2005). After re-running each  
258 model parametrization (different  $\tau$  values) to obtain those bank-full discharge values, we  
259 calculated  $\text{floodh}_{95\text{th}}$  over the simulation period for each grid cell (Table 1). This value is  
260 assumed to represent the water level over the river banks at which the maximum horizontal  
261 extent of floodplain inundation is reached. We then ran the model for a final time and validated  
262 the outputs against discharge data at Brazzaville (Cochonneau et al., 2006, Fig. 1). This  
263 procedure was repeated iteratively with the ISIMIP2b climate forcing, modifying the  $\tau$  value  
264 of each reservoir in order to find the best performing parametrization.

265 We firstly compared simulated versus observed discharge at Brazzaville (NSE, RMSE, Table  
266 2), before using the data of Bouillon et al. (2014) to further validate discharge at Bangui (Fig.  
267 1) on the main tributary Oubangui. In addition, we compared the simulated seasonality of  
268 flooded area against the satellite derived dataset GIEMS (Prigent et al., 2007; Becker et al.,  
269 2018), within the Cuvette Centrale wetlands (Fig. 1).

## 270 **2.4 Simulation set-up**

271 A list of the main forcing files used, along with data sources, is presented in Table 1. The  
272 derivation of the floodplains and swamp (MFF & MFS) is described in section 2.2 while the  
273 calculation of “bankfull discharge” ( $\text{streamr}_{50\text{th}}$ ) and “95th percentile of water table height over  
274 flood plain” ( $\text{floodh}_{95\text{th}}$ ) (Table 1) is described in section 2.3.

### 275 **2.4.1 Soil carbon spin up**

276 ORCHILEAK includes a soil module, primarily derived from ORCHIDEE-SOM (Camino  
277 Serrano, 2018). The soil module has 3 different pools of soil DOC; the passive, slow and active  
278 pool and these are defined by their source material and residence times ( $\tau_{\text{carbon}}$ ). ORCHILEAK  
279 also differentiates between flooded and non-flooded soils; decomposition rates of DOC, SOC  
280 and litter being reduced (3 times lower) in flooded soils. In order for the soil C pools to reach  
281 steady state, we spun-up the model for around 9,000 years, with fixed land-use representative  
282 of 1861, and looping over the first 30 years of the ISMSIP2b climate forcing data (1861-1890).  
283 During the first 2,000 years of spin-up, we ran the model with an atmospheric  $\text{CO}_2$   
284 concentration of  $350 \mu\text{atm}$  and default soil C residence times ( $\tau_{\text{carbon}}$ ) halved, which allowed it  
285 to approach steady-state more rapidly. Following this, we ran the model for a further 7,000  
286 years reverting to the default  $\tau_{\text{carbon}}$  values. At the end of this process, the soil C pools had  
287 reached approximately steady state;  $<0.02\%$  change in each pool over the final century of the  
288 spin-up.

### 289 **2.4.2 Transient simulations**

290 After the spin-up, we ran a historical simulation from 1861 until the present day, 2005 in the  
291 case of the ISIMIP2b climate forcing data. We then ran a future simulation until 2099, using  
292 the final year of the historical simulation as a restart file. In both of these simulations, climate,  
293 atmospheric  $\text{CO}_2$  and land-cover change were prescribed as fully transient forcings according  
294 to the RCP6.0 scenario. For climate variables, we used the IPSL-CM5A-LR model outputs for

295 RCP 6.0, bias corrected by the ISIMIP2b procedure (Frieler et al., 2017; Lange et al., 2017),  
296 while land-use change was taken from the 5th Coupled Model Intercomparison Project  
297 (CMIP5). As our aim is to investigate long-term trends, we calculated 30-years running means  
298 of simulated C flux outputs in order to smooth interannual variations. RCP 6.0 is an emissions  
299 pathway that leads to a “stabilization of radiative forcing at 6.0 Watts per square meter ( $\text{Wm}^{-2}$ )  
300 in the year 2100 without exceeding that value in prior years” (Masui et al., 2011). It is  
301 characterised by intermediate energy intensity, substantial population growth, mid-high C  
302 emissions, increasing cropland area to 2100 and decreasing natural grassland area (van Vuuren  
303 et al., 2011). In the paper which describes the development of the future land use change  
304 scenarios under RCP 6.0 (Hurtt et al., 2011), it is shown that land use change is highly sensitive  
305 to land use model assumptions, such as whether or not shifting cultivation is included. The  
306 LUH1 reconstruction for instance indicates shifting cultivation affecting all of the tropics with  
307 a residence time of agriculture of 15 years, whereas the review from Heinemann et al. (2017)  
308 revised downwards the area of this type of agriculture, with generally low values in Congo,  
309 except in the North East and South East, but suggested a shorter turnover of agriculture of two  
310 years only. In view of such uncertainties, we did not include shifting agriculture in the model.  
311 Moreover, there is considerable uncertainty associated with the effect of future land-use change  
312 in Africa (Hurtt et al., 2011). We chose RCP 6.0 as it represents a no mitigation (mid-high  
313 emissions) scenario. Moreover, the ISIMIP2b data only provided two RCPs at the time we  
314 performed the simulations; RCP 2.6 (low emission) and RCP 6.0.

315 With the purpose of evaluating separately the effects of land-use change, climate change, and  
316 rising atmospheric  $\text{CO}_2$ , we ran a series of factorial simulations. In each simulation, one of  
317 these factors was fixed at its 1861 level (the first year of the simulation), or in the case of fixed  
318 climate change, we looped over the years 1861-1890. The outputs of these simulations (also  
319 30-year running means) were then subtracted from the outputs of the main simulation (original

320 run with all factors varied) so that we could determine the contribution of each driver (Fig. 10,  
 321 Table 1).

<b>Variable</b>	<b>Spatial resolution</b>	<b>Temporal resolution</b>	<b>Data source</b>
Rainfall, incoming shortwave and longwave radiation, air temperature, relative humidity and air pressure (close to surface), wind speed (10 m above surface)	1°	1 day	ISIMIP2b, IPSL-CM5A-LR model outputs for RCP6.0 (Frieler et al., 2017)
Land cover (and change)	0.5°	annual	LUH-CMIP5
Poor soils	0.5°	annual	Derived from HWSO v 1.1 (FAO/IIASA/ISRIC/ISS-CAS/JRC, 2009)
Stream flow directions	0.5°	annual	STN-30p (Vörösmarty et al., 2000)
Floodplains and swamps fraction in each grid (MFF & MFS)	0.5°	annual	derived from the wetland high resolution data of Gumbrecht et al. (2017)
River surface areas	0.5°	annual	Lauerwald et al. (2015)
Bankfull discharge (streamr <sub>50th</sub> )	1°	annual	derived from calibration with ORCHILEAK (see section 2.3)
95th percentile of water table height over flood plain (floodh <sub>95th</sub> )	1°	annual	derived from calibration with ORCHILEAK (see section 2.3)

## 322 **2.5 Evaluation and analysis of simulated fluvial C fluxes**

323 We first evaluated DOC concentrations and  $p\text{CO}_2$  at several locations along the Congo  
 324 mainstem (Fig. 1), and on the Oubangui river against the data of Borges et al. (2015<sup>b</sup>) and  
 325 Bouillon et al. (2012, 2014) We also compared the various simulated components of the net C  
 326 balance (e.g. NPP) of the Congo against values described in the literature (Williams et al.,  
 327 2007; Lewis et al., 2009; Verhegghen et al., 2012; Valentini et al., 2014; Yin et al., 2017). In  
 328 addition, we assessed the relationship between the interannual variation in present day (1981-  
 329 2010) C fluxes of the Congo basin and variation in temperature and rainfall. This was done  
 330 through linear regression using STATISTICA™. We found trends in several of the fluxes over  
 331 the 30-year period (1981-2010) and thus detrended the time series with the “Detrend” function,  
 332 part of the “SpecsVerification” package in R (R Core Team 2013), before undertaking the  
 333 statistical analysis focused on the climate drivers of inter-annual variability.



## 334 **2.6 Calculating the net carbon balance of the Congo basin**

335 We calculated Net Ecosystem Production (NEP) by summing the terrestrial and aquatic C  
336 fluxes of the Congo basin (Eq. 1), while we incorporated disturbance fluxes (Land-use change  
337 flux and harvest flux) to calculate Net Biome Production (NBP) (Eq. 2). Positive values of  
338 NBP and NEP equate to a net terrestrial C sink.

339 NEP is defined as follows:

$$340 \quad \quad \quad NEP = NPP + TF - SHR - FCO_2 - LE_{Aquatic} \quad (1)$$

341 Where *NPP* is terrestrial net primary production, *TF* is the throughfall flux of DOC from the  
342 canopy to the ground, *SHR* is soil heterotrophic respiration (only that evading from the *terra-*  
343 *firme* soil surface); *FCO<sub>2</sub>* is CO<sub>2</sub> evasion from the water surface and *LE<sub>Aquatic</sub>* is the lateral  
344 export flux of C (DOC + dissolved CO<sub>2</sub>) to the coast. NBP is equal to NEP except with the  
345 inclusion of the C lost (or possibly gained) via land use change (*LUC*) and crop harvest (*HAR*).  
346 Wood harvest is not included for logging and forestry practices, but during deforestation LUC,  
347 a fraction of the forest biomass is harvested and channelled to wood product pools with  
348 different decay constants. *LUC* includes land conversion fluxes and the lateral export of wood  
349 products biomass, that is, assuming that wood products from deforestation are not consumed  
350 and released as CO<sub>2</sub> over the Congo, but in other regions:

$$351 \quad \quad \quad NBP = NEP - (LUC + HAR) \quad (2)$$

352

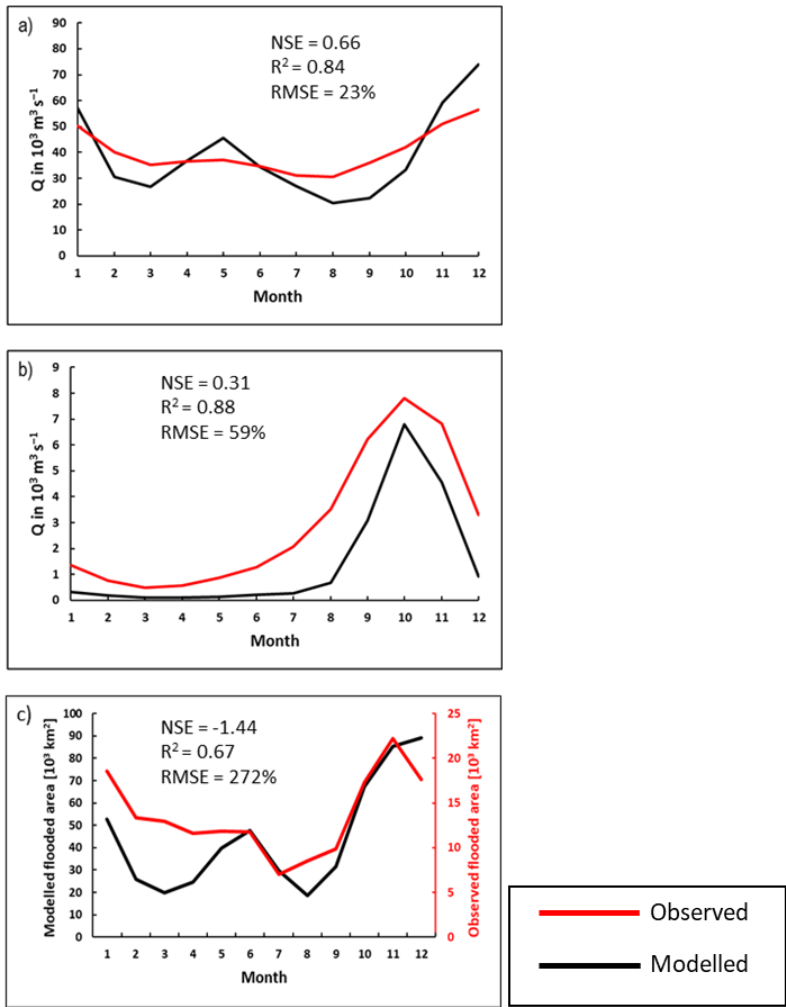
## 353 **3. Results**

### 354 **3.1 Simulation of hydrology and aquatic carbon fluxes**

355 The final model configuration is able to closely reproduce the mean monthly discharge at  
356 Brazzaville (Fig. 4 a), Table 2) and captures the seasonality moderately well (Fig. 4 a, Table 2,

357 RMSE =23%,  $R^2$  =0.84 versus RMSE= 29% and  $R^2$  =0.23 without calibration, Table A1). At  
358 Bangui on the Oubangui River (Fig. 1), the model is able to closely recreate observed  
359 seasonality (Fig. 4 b), RMSE =59%,  $R^2$  =0.88) but substantially underestimates the mean  
360 monthly discharge, our value being only 50% of the observed. We produce reasonable NSE  
361 values of 0.66 and 0.31 for Brazzaville and Bangui respectively, indicating that the model is  
362 moderately accurate in its simulation of seasonality.

363 We also evaluated the simulated seasonal change in flooded area in the central (approx.  
364 200,000 km<sup>2</sup>, Fig. 1) part of the Cuvette Centrale wetlands against the GIEMS inundation  
365 dataset (1993-2007, maximum inundation minus minimum or permanent water bodies, Prigent  
366 et al., 2007; Becker et al., 2018). While our model is able to represent the seasonality in flooded  
367 area relatively well ( $R^2$  =0.75 Fig. 4 c), it considerably overestimates the magnitude of flooded  
368 area relative to GIEMS (Fig. 4 c, Table 2). However, the dataset that we used to define the  
369 MFF and MFS forcing files (Gumbricht et al., 2017) is produced at a higher resolution than  
370 GIEMS and will capture smaller wetlands than the GIEMS dataset, and thus the greater flooded  
371 area is to be expected. GIEMS is also known to underestimate inundation under vegetated areas  
372 (Prigent et al., 2007; Papa et al., 2010) and has difficulties to capture small inundated areas  
373 (Prigent et al., 2007; Lauerwald et al., 2017). Indeed, with the GIEMS data we produce an  
374 overall flooded area for the Congo Basin of just 3%, less than one-third of that produced with  
375 the Gumbricht dataset (Gumbricht et al., 2017) or the GLWD (Lehner, & Döll, P.,2004). As  
376 such, it is to be expected that there is a large RMSE (272%, Table 2) between simulated flooded  
377 area and GIEMS; more importantly, the seasonality of the two is highly correlated ( $R^2$  = 0.67,  
378 Table 2).



380

381 **Figure 4: Seasonality of simulated versus observed discharge at a) Brazzaville on the**  
 382 **Congo (Cochonneau et al., 2006), b) Bangui on the Oubangui (Bouillon et al., 2014) 1990-**  
 383 **2005 monthly mean and c) flooded area in the central (approx. 200,000 km<sup>2</sup>) area of the**  
**Cuvette Centrale wetlands versus GIEMS (1993-2007, Becker et al., 2018). The observed**  
 384 **flooded area data represents the maximum minus minimum (permanent water bodies**  
**such as rivers) GIEMS inundation. See Figure 1 for locations.**

384

**Table 2: Performance statistics for modelled versus observed seasonality of discharge and flooded area in Cuvette Centrale. Observed flooded area is from GIEMS (Papa et al., 2010, Becker et al., 2018).**

Station	RSME	NSE	R <sup>2</sup>	Simulated mean monthly discharge (m <sup>3</sup> s <sup>-1</sup> )	Observed mean monthly discharge (m <sup>3</sup> s <sup>-1</sup> )
Brazzaville	23%	0.66	0.84	38,944	40,080
Bangui	59%	0.31	0.88	1,448	2,923
				Simulated mean monthly flooded area (10 <sup>3</sup> km <sup>2</sup> )	Observed mean monthly flooded area (10 <sup>3</sup> km <sup>2</sup> )
Flooded area (Cuvette Centrale)	272%	-1.44	0.67	44	14

385

386 In Figure 5, we compare simulated DOC concentrations at six locations (Fig. 1) along the  
387 Congo River and Oubangui tributary, against the observations of Borges et al. (2015<sup>b</sup>). We  
388 show that we can recreate the spatial variation in DOC concentration within the Congo basin  
389 relatively closely with an R<sup>2</sup> of 0.74 and an RMSE of 24% (Fig. 5). We are also able to  
390 simulate the broad spatial pattern of pCO<sub>2</sub> measured in the main-stem Congo reported by  
391 Borges et al. (2019). During high flow season (mean of 6 consecutive months of highest flow,  
392 2009-2019-to account for interannual variation) we simulate a mean pCO<sub>2</sub> of 3,373 ppm and  
393 5,095 ppm at Kisangani and Kinshasa (Brazzaville) respectively, compared to the observed  
394 values of 2,424 ppm and 5,343 ppm during high water (measured in December 2013, Borges  
395 et al., 2019) (Table 3). Similarly, during low flow season (mean of 6 consecutive months of  
396 lowest flow, 2009-2019) we simulate a mean pCO<sub>2</sub> of 1,563 ppm and 2,782 ppm at Kisangani  
397 and Kinshasa respectively, compared to the observed values of 1,670 ppm and 2,896 ppm  
398 during falling water (June 2014, Borges et al., 2019) (Table 3).

399

400 While we are able to recreate observed spatial differences in DOC and  $p\text{CO}_2$ , as well as broad  
401 seasonal variations, we are not able to correctly predict the exact timing of the simulated  
402 highs and lows, a reflection of not fully capturing the hydrological seasonality. For example,  
403 our mean June  $p\text{CO}_2$  at Kinshasa (Brazzaville) is 4,470 ppm, while Borges et al measured a  
404 mean of 2,896 ppm (Table 3). However, our value for July of 2,621 ppm is much closer, and  
405 moreover our mean value for December of 5,154 ppm is relatively close to the observed  
406 value of 5,343 ppm. Similarly, we fail to predict the timing of the June falling water at  
407 Kisangani (Table 3).

408 In Figure 6, we compare simulated  $p\text{CO}_2$  against the observed monthly time series at Bangui  
409 on the Oubangui River (Bouillon et al., 2012 & 2014), as far as we are aware the longest time  
410 series of  $p\text{CO}_2$  published (and accessible) from the Congo basin, spanning March 2010 to  
411 March 2012 (with only the single month of June 2010 missing). Again, while the model fails  
412 to correctly predict the precise timing of the peak as with the Kinshasa and Kisangani  
413 datasets the broad seasonal variation in  $p\text{CO}_2$  is captured, with the observed and modelled  
414 times series ranging from 227- 4040 ppm and 415- 2928 ppm, respectively (Fig. 6).

415

416

417

418

419

420

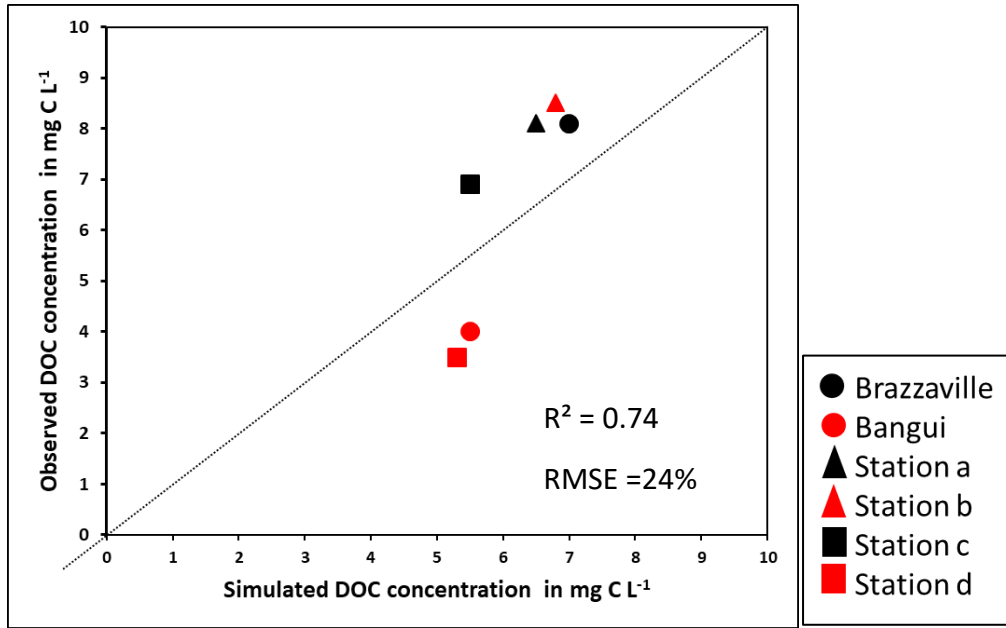
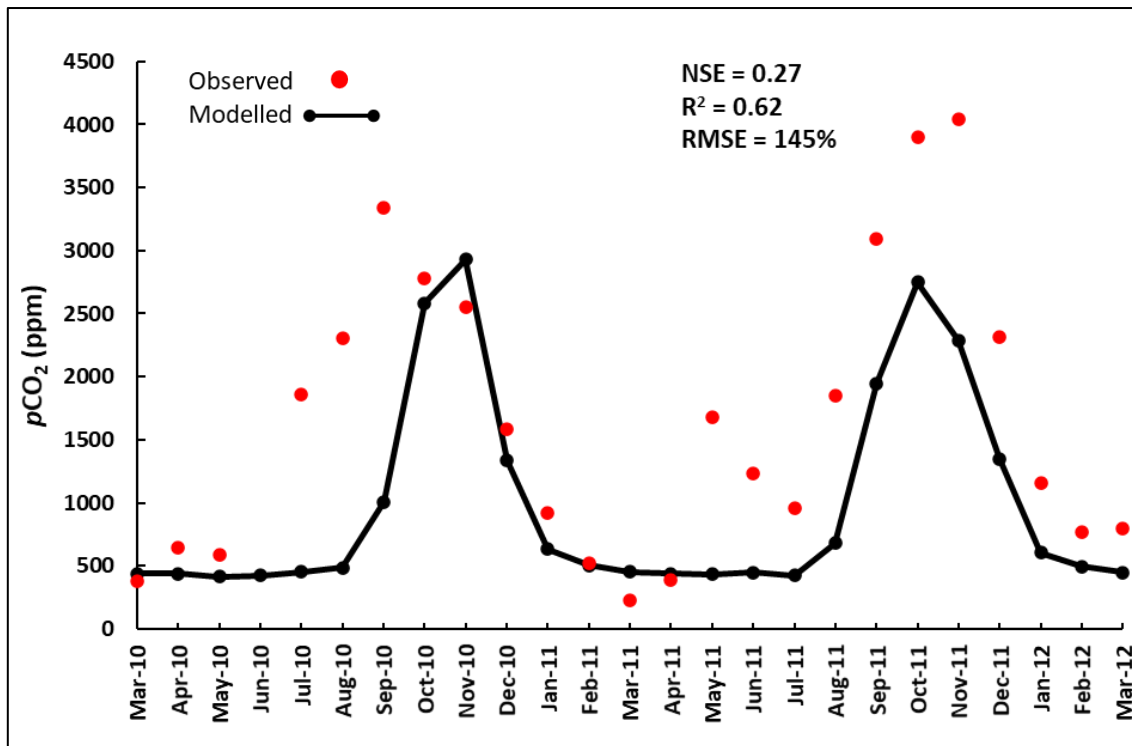


**Figure 5: Observed (Borges et al., 2015<sup>a</sup>) versus simulated DOC concentrations at several sites along the Congo and Oubangui rivers. See Fig. 1 for locations. The simulated and observed DOC concentrations represent the median values across the particular sampling period at each location detailed in Borges et al. (2015<sup>a</sup>).**

421

Location	Observed $p\text{CO}_2$ highwater (December 2013)	Modelled $p\text{CO}_2$ highwater (December Mean 2009-2019)	Modelled $p\text{CO}_2$ high flow season (mean of 6 consecutive months of highest flow 2009-2019)	Observed $p\text{CO}_2$ falling water (June 2014)	Modelled $p\text{CO}_2$ falling water (June mean 2009-2019)	Modelled $p\text{CO}_2$ low flow season (mean of 6 consecutive months of lowest flow 2009-2019)
Kinshasa (Brazzaville)	5,343	5,154	5,095	2,896	4,470	2,782
Kisangani	2,424	2,166	3,373	1,670	3,126	1,563

422



424

425

**Figure 6: Time series of observed *versus* simulated  $p\text{CO}_2$  at Bangui on the River Oubangui. Observed data is from Bouillon et al., 2012 and Bouillon et al., 2014.**

426

### 427 3.2 Carbon fluxes along the Congo basin for the present day

428 For the present day (1981-2010) we estimate a mean annual terrestrial net primary production

429 (NPP) of  $5,800 \pm 166$  (standard deviation, SD)  $\text{Tg C yr}^{-1}$  (Fig. 7), corresponding to a mean areal

430 C fixation rate of approximately  $1,500 \text{ g C m}^{-2} \text{ yr}^{-1}$  (Fig. 8 a). We find a significant positive

431 correlation between the interannual variation of NPP and rainfall (detrended  $R^2 = 0.41$ ,  $p < 0.001$ ,

432 Table A2) and a negative correlation between annual NPP and temperature (detrended  $R^2 =$

433  $0.32$ ,  $p < 0.01$ , Table A2). We also see considerable spatial variation in NPP across the Congo

434 Basin (Fig.8 a).

435 We simulate a mean soil heterotrophic respiration (SHR) of  $5,300 \pm 99 \text{ Tg C yr}^{-1}$  across the

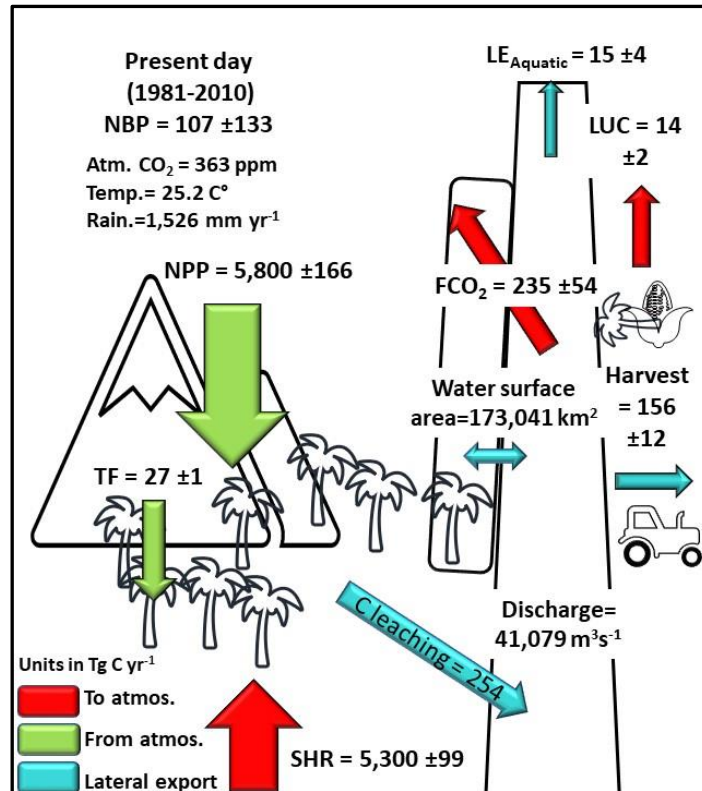
436 Congo basin (Fig. 7). Contrary to NPP, interannual variation in annual SHR is positively

437 correlated with temperature (detrended  $R^2=0.57$ ,  $p<0.0001$ , Table A2) and inversely correlated  
438 with rainfall (detrended  $R^2=0.10$ ), though the latter relationship is not significant ( $p>0.05$ ).  
439 We estimate a mean annual aquatic  $\text{CO}_2$  evasion rate of  $1,363 \pm 83 \text{ g C m}^{-2} \text{ yr}^{-1}$ , amounting to  
440 a total of  $235 \pm 54 \text{ Tg C yr}^{-1}$  across the total water surfaces of the Congo basin (Fig. 7) and  
441 attribute 85% of this flux to flooded areas, meaning that only  $32 \text{ Tg C yr}^{-1}$  is evaded directly  
442 from the river surface. Interannual variation in aquatic  $\text{CO}_2$  evasion (1981-2010) shows a  
443 strong positive correlation with rainfall (detrended  $R^2=0.75$ ,  $p<0.0001$ , Table A2) and a weak  
444 negative correlation with temperature (detrended  $R^2=0.09$ , not significant,  $p>0.05$ ). Aquatic  
445  $\text{CO}_2$  evasion also exhibits substantial spatial variation (Fig.8, d), displaying a similar pattern to  
446 both terrestrial DOC leaching ( $\text{DOC}_{\text{inp}}$ ) ( $R^2=0.81$ ,  $p<0.0001$ , Fig.8, b) as well as terrestrial  
447  $\text{CO}_2$  leaching ( $\text{CO}_{2\text{inp}}$ ) ( $R^2=0.96$ ,  $p<0.0001$ , Fig.8, c) into the aquatic system, but not terrestrial  
448 NPP ( $R^2=0.01$ ,  $p<0.05$ , Fig.8, a). We simulate a mean annual flux of DOC throughfall from  
449 the canopy of  $27 \pm 1 \text{ Tg C yr}^{-1}$  and C (DOC + dissolved  $\text{CO}_2$ ) export flux to the coast of  $15 \pm 4$   
450  $\text{Tg C yr}^{-1}$  (Fig. 7).

451 For the present day (1981-2010) we estimate a mean annual net ecosystem production (NEP)  
452 of  $277 \pm 137 \text{ Tg C yr}^{-1}$  and a net biome production (NBP) of  $107 \pm 133 \text{ Tg C yr}^{-1}$  (Fig. 7).  
453 Interannually, both NEP and NBP exhibit a strong inverse correlation with temperature  
454 (detrended NEP  $R^2=0.55$ ,  $p<0.0001$ , detrended NBP  $R^2=0.54$ ,  $p<0.0001$ ) and weak positive  
455 relationship with rainfall (detrended NEP  $R^2=0.16$ ,  $p<0.05$ , detrended NBP  $R^2=0.14$ ,  $p<0.05$ ).  
456 Furthermore, we simulate a present day (1981-2010) living biomass of  $41 \pm 1 \text{ Pg C}$  and a total  
457 soil C stock of  $109 \pm 1 \text{ Pg C}$ .

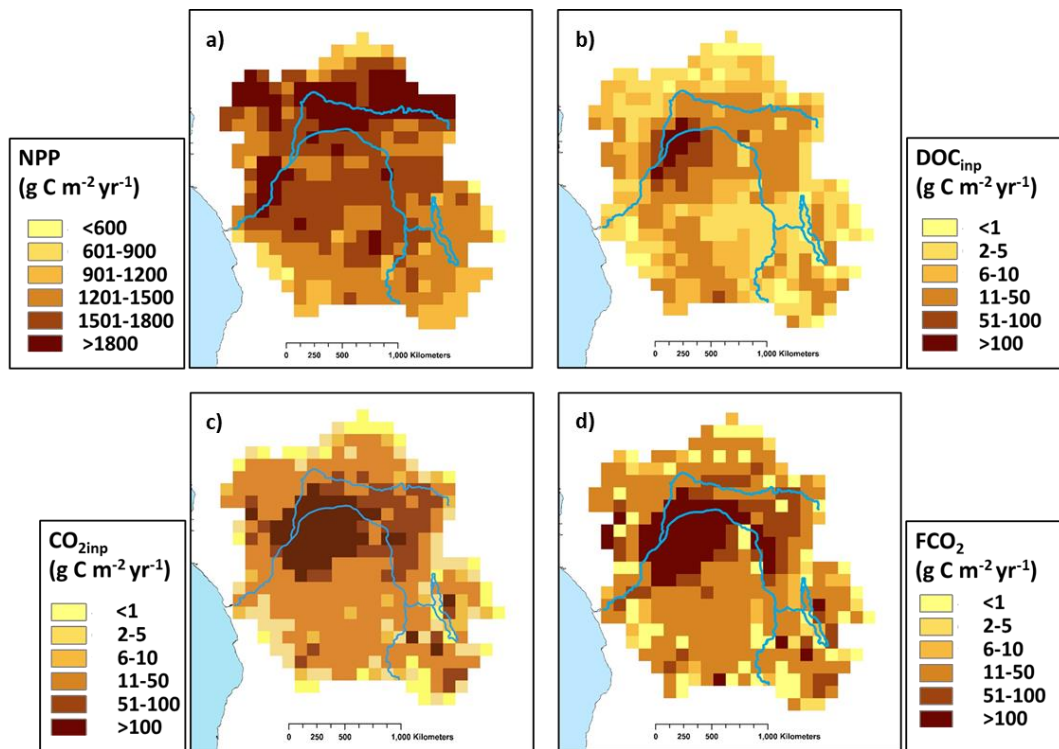
458





459

**Figure 7: Annual C budget (NBP) for the Congo basin for the present day (1981-2010) simulated with ORCHILEAK, where NPP is terrestrial net primary productivity, TF is throughfall, SHR is soil heterotrophic respiration, FCO<sub>2</sub> is aquatic CO<sub>2</sub> evasion, LOAC is C leakage to the land-ocean aquatic continuum (FCO<sub>2</sub> + LE<sub>Aquatic</sub>), LUC is flux from Land-use change, and LE<sub>Aquatic</sub> is the export C flux to the coast. Range represents the standard deviation (SD) from 1981-2010.**



460

**Figure 8: Present day (1981-2010) spatial distribution of a) terrestrial net primary productivity (NPP), b) dissolved organic carbon export from soils and floodplain vegetation into the aquatic system ( $DOC_{inp}$ ), c)  $CO_2$  leaching from soils and floodplain vegetation into the aquatic system ( $CO_{2inp}$ ) and d) aquatic  $CO_2$  evasion ( $FCO_2$ ). Main rivers in blue. All at a resolution of  $1^\circ$**

461

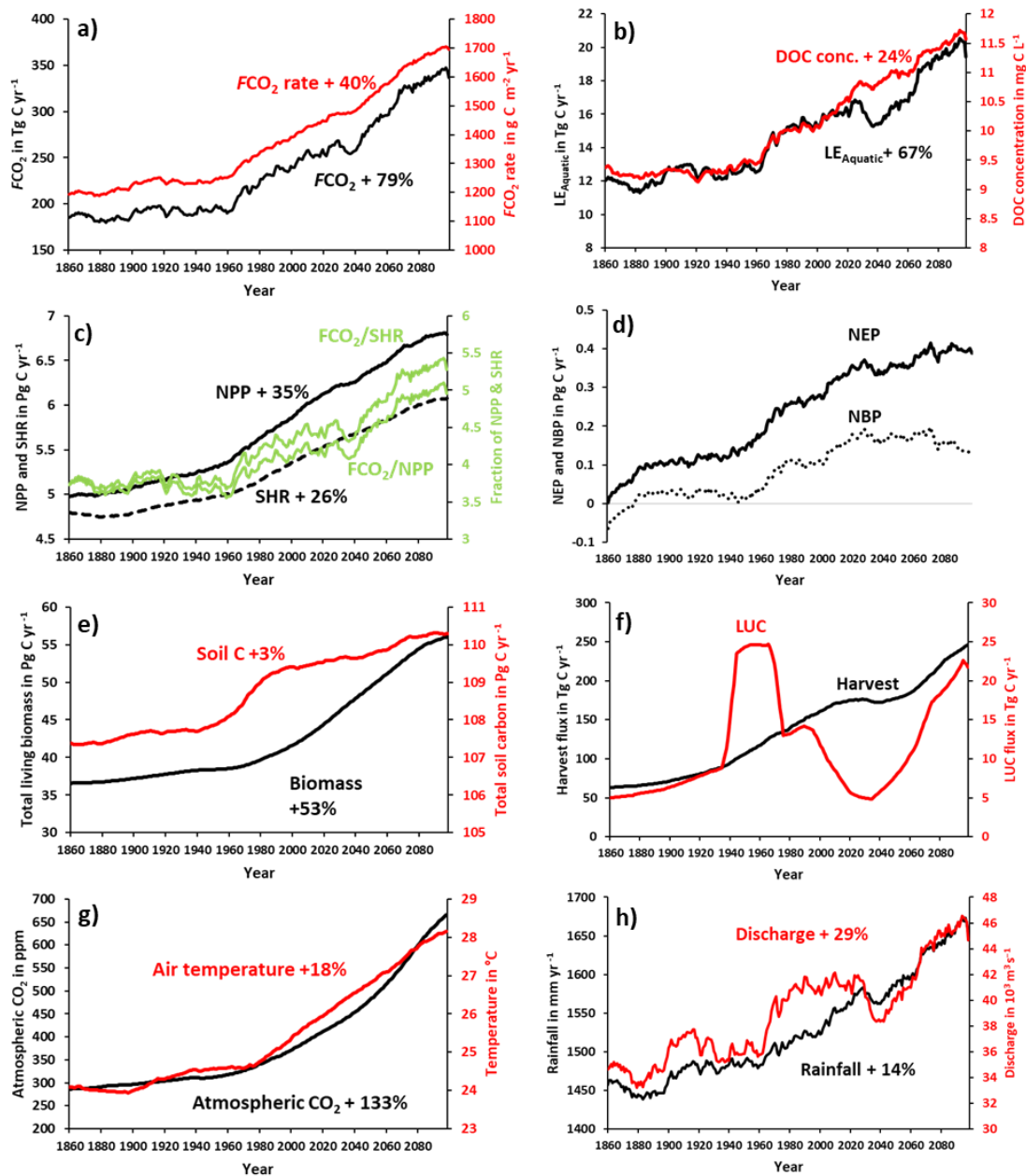
### 462 **3.3 Long-term temporal trends in carbon fluxes**

463 We find an increasing trend in aquatic  $CO_2$  evasion (Fig. 9 a) throughout the simulation period,  
 464 rising slowly at first until the 1960s when the rate of increase accelerates. In total  $CO_2$  evasion  
 465 rose by 79% from 186 Tg C yr<sup>-1</sup> at the start of the simulation (1861-1890 mean) (Fig. 10) to  
 466 333 Tg C yr<sup>-1</sup> at the end of this century (2070-2099 mean, Fig. 10), while the increase until the  
 467 present day (1981-2010 mean) is +26 % (to 235 Tg C yr<sup>-1</sup>), though these trends are not uniform  
 468 across the basin (Fig A1). The lateral export flux of C to the coast ( $LE_{Aquatic}$ ) follows a similar  
 469 relative change (Fig. 9b), rising by 67% in total, from 12 Tg C yr<sup>-1</sup> (Fig. 10) to 15 Tg C yr<sup>-1</sup> for  
 470 the present day, and finally to 20 Tg C yr<sup>-1</sup> (2070-2099 mean, Fig. 10). This is greater than the  
 471 equivalent increase in DOC concentration (24%, Fig. 9b) due to the concurrent rise in rainfall  
 472 (by 14%, Fig 9h) and in turn discharge (by 29%, Fig. 9h).

473 Terrestrial NPP and SHR also exhibit substantial increases of 35% and 26% respectively across  
474 the simulation period and similarly rise rapidly after 1960 (Fig. 9c). NEP, NBP (Fig. 9d) and  
475 living biomass (Fig. 9 e) follow roughly the same trend as NPP, but NEP and NBP begin to  
476 slow down or even level-off around 2030 and in the case of NBP, we actually simulate a  
477 decreasing trend over approximately the final 50 years. Interestingly, the proportion of NPP  
478 lost to the LOAC also increases from approximately 3% to 5% (Fig. 9c). We also find that  
479 living biomass stock increases by a total of 53% from 1861 to 2099. Total soil C also increases  
480 over the simulation but only by 3% from 107 to 110 Pg C yr<sup>-1</sup> (Fig. 9e). Emissions from land-  
481 use change (LUC) show considerable decadal fluctuation increasing rapidly in the second half  
482 of the 20<sup>th</sup> century and decreasing in the mid-21<sup>st</sup> century before rising again towards the end  
483 of the simulation (Fig. 9f). The harvest flux (Fig. 9f) rises throughout the simulation with the  
484 exception of a period in the mid-21<sup>st</sup> century during which it stalls for several decades. This is  
485 reflected in the change in land-use areas from 1861- 2099 (Fig. A2, Table A3) during which  
486 the natural forest and grassland PFTs marginally decrease while both C<sub>3</sub> and C<sub>4</sub> agricultural  
487 grassland PFTs increase.

488

489



491 **Figure 9: Simulation results for various C fluxes and stocks from 1861-2099, using IPSL-**  
 492 **CM5A-LR model outputs for RCP 6.0 (Frierler et al., 2017). All panels except for atmospheric**  
 493 **CO<sub>2</sub>, biomass and soil C correspond to 30-year running means of simulation outputs. This**  
 494 **was done in order to suppress interannual variation, as we are interested in longer-term**  
 495 **trends.**

496 **3.4 Drivers of simulated trends in carbon fluxes**

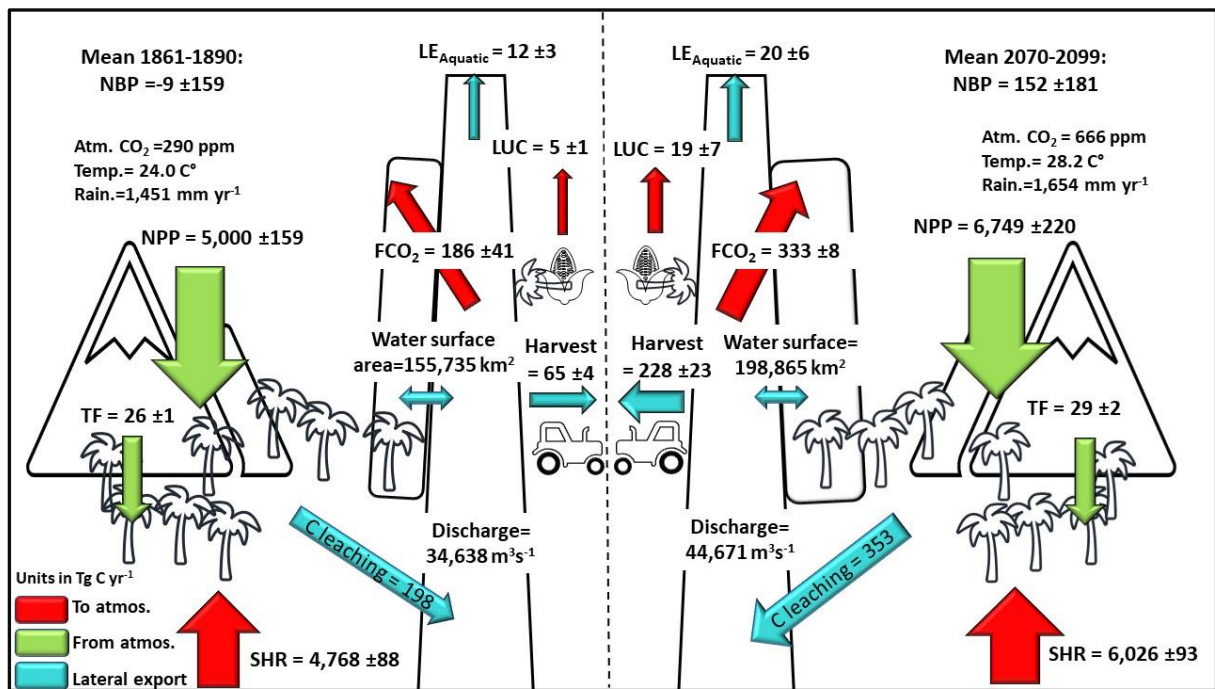
497 The dramatic increase in the concentration of atmospheric CO<sub>2</sub> (Fig. 9 g) and subsequent  
 498 fertilization effect on terrestrial NPP has the greatest overall impact on all of the fluxes across

499 the simulation period (Fig. 11). It is responsible for the vast majority of the growth in NPP,  
500 SHR, aquatic CO<sub>2</sub> evasion and flux of C to the coast (Fig. 11 a, b, c & d). The effect of LUC  
501 on these four fluxes is more or less neutral, while the impact of climate change is more varied.  
502 The aquatic fluxes (Fig. 11 c, d) respond positively to an acceleration in the increase of both  
503 rainfall (and in turn discharge, Fig. 9 h) and temperature (Fig. 9 g) starting around 1970. From  
504 around 2020, the impact of climate change on the lateral flux of C to the coast (Fig 11 d) reverts  
505 to being effectively neutral, likely a response to a slowdown in the rise of rainfall and indeed a  
506 decrease in discharge (Fig 9 h), as well as perhaps the effect of temperature crossing a  
507 threshold. The response of the overall loss of terrestrial C to the LOAC (i.e. the ratio of  
508 LOAC/NPP, Fig. 11 e) is relatively similar to the response of the individual aquatic fluxes but  
509 crucially, climate change exerts a much greater impact, contributing substantially to an increase  
510 in the loss of terrestrial NPP to the LOAC in the 1960s, and again in the second half of the 21<sup>st</sup>  
511 century. These changes closely coincide with the pattern of rainfall and in particular with  
512 changes in discharge (Fig. 9 h).

513 Overall temperature and rainfall increase by 18% and 14% from 24°C to 28°C and 1457mm to  
514 1654mm respectively, but in Fig. A2 one can see that this increase is non-uniform across the  
515 basin. Generally speaking, the greatest increase in temperature occurs in the south of the basin  
516 while it is the east that sees the largest rise in rainfall (Fig. A2). Land-use changes are similarly  
517 non-uniform (Fig. A2).

518 The response of NBP and in NEP (Fig.11 f, g) to anthropogenic drivers is more complex. The  
519 simulated decrease in NBP towards the end of the run is influenced by a variety of factors;  
520 LUC and climate begin to have a negative effect on NBP (contributing to a decrease in NBP)  
521 at a similar time while the positive impact (contributing to an increase in NBP) of atmospheric  
522 CO<sub>2</sub> begins to slow down and eventually level-off (Fig.11 g). LUC continues to have a positive  
523 effect on NEP (Fig.11 f) due to the fact that the expanding C<sub>4</sub> crops have a higher NPP than

524 forests, while it has an overall negative effect on NBP at the end of the simulation due to the  
 525 inclusion of emissions from crop harvest.



526

527 **Figure 10: Annual C budget (NBP) for the Congo basin for; left, the Year 1861 and right, the**  
 528 **Year 2099, simulated with ORCHILEAK. NPP is terrestrial net primary productivity, TF is**  
 529 **throughfall, SHR is soil heterotrophic respiration, FCO<sub>2</sub> is aquatic CO<sub>2</sub> evasion, LOAC is C**  
 530 **leakage to the land-ocean aquatic continuum (FCO<sub>2</sub> + LE<sub>Aquatic</sub>), LUC is flux from Land-use**  
 531 **change, and LE<sub>Aquatic</sub> is the export C flux to the coast. Range represents the standard deviation**  
 532 **(SD).**

533

534

535

536

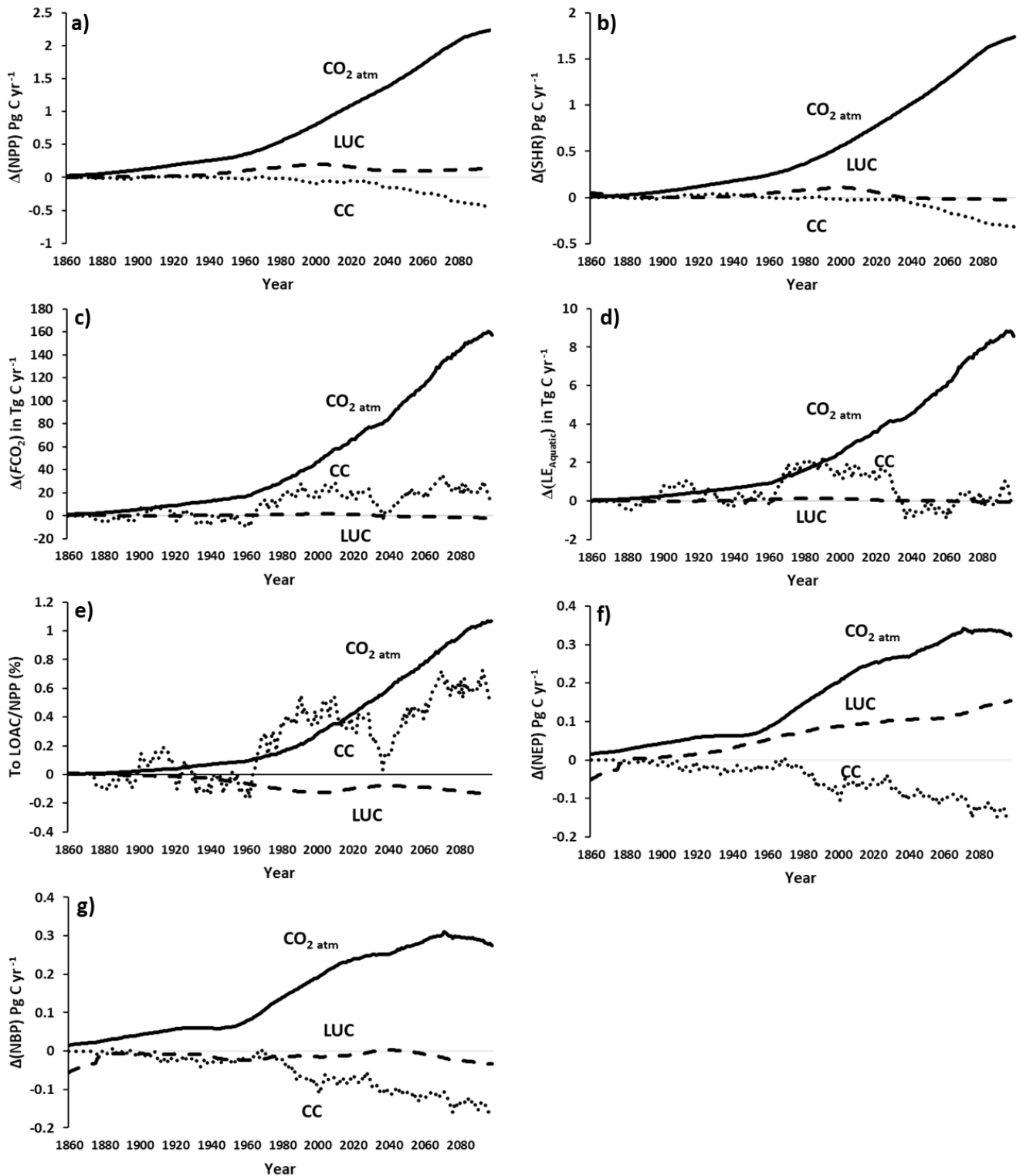


Figure 11: Contribution of anthropogenic drivers; atmospheric CO<sub>2</sub> concentration (CO<sub>2 atm</sub>), climate change (CC) and land use change (LUC) to changes in the various carbon fluxes along the Congo Basin, under IPSL-CM5A-LR model outputs for RCP 6.0 (Frieler et al., 2017).

## 540 **4. Discussion**

### 541 **4.1 Congo basin carbon balance**

542 We simulate a mean present-day terrestrial NPP of approximately  $1,500 \text{ g C m}^{-2} \text{ yr}^{-1}$  (Fig. 6),  
543 substantially larger than the MODIS derived value of around  $1,000 \text{ g C m}^{-2} \text{ yr}^{-1}$  from Yin et al.  
544 (2017) across central Africa, though it is important to note that satellite derived estimates of  
545 NPP can underestimate the impact of  $\text{CO}_2$  fertilization, namely its positive effect on  
546 photosynthesis (De Kauwe et al., 2016; Smith et al., 2019). Our stock of the present-day living  
547 biomass of 41.1 Pg C is relatively close to the total Congo vegetation biomass of 49.3 Pg C  
548 estimated by Verhegghen et al. (2012) based on the analysis of MERIS satellite data. Moreover,  
549 our simulated Congo Basin soil C stock of  $109 \pm 1.1 \text{ Pg C}$  is consistent with the approximately  
550 120-130 Pg C across Africa between the latitudes  $10^\circ\text{S}$  to  $10^\circ\text{N}$  in the review of Williams et  
551 al. (2007), between which the Congo represents roughly 70% of the land area. Therefore, their  
552 estimate of soil C stocks across the Congo only, would likely be marginally smaller than ours.  
553 It is also important to note that neither estimate of soil C stocks explicitly take into account the  
554 newly discovered peat store of 30 Pg C (Dargie et al., 2017) and therefore both are likely to  
555 represent conservative values. In addition, Williams et al. (2007) estimate the combined fluxes  
556 from conversion to agriculture and cultivation to be around  $100 \text{ Tg C yr}^{-1}$  in tropical Africa  
557 (largely synonymous with the Congo Basin), which is relatively close to our present-day  
558 estimate of harvesting + land-use change flux of  $170 \text{ Tg C yr}^{-1}$ .

559 Our results suggest that  $\text{CO}_2$  evasion from the water surfaces of the Congo is sustained by the  
560 transfer of dissolved  $\text{CO}_2$  and DOC with 226 Tg C and 73 Tg C, respectively, from wetland  
561 soils and vegetation to the aquatic system each year (1980-2010, Fig. 8). Moreover, we find  
562 that a disproportionate amount of this transfer occurs within the Cuvette Centrale wetland (Fig.  
563 1, Fig. 8) in the centre of the basin, in agreement with a recent study by Borges et al. (2019).  
564 In our study, this is due to the large areal proportion of inundated land, facilitating the exchange



565 between soils and aquatic systems. Borges et al. (2019) conducted measurements of DOC and  
566  $p\text{CO}_2$ , amongst other chemical variables, along the Congo mainstem and its tributaries from  
567 Kinshasa in the West of the basin (beside Brazzaville, Fig. 1) through the Cuvette Centrale to  
568 Kisangani in the East (close to station d in Fig. 1). They found that both DOC and  $p\text{CO}_2$   
569 approximately doubled from Kisangani downstream to Kinshasa (Table 3), and demonstrated  
570 that this variation is overwhelmingly driven by fluvial-wetland connectivity, highlighting the  
571 importance of the vast Cuvette Centrale wetland in the aquatic C budget of the Congo basin.

572 Our estimate of the integrated present-day aquatic  $\text{CO}_2$  evasion from the river surface of the  
573 Congo basin ( $32 \text{ Tg C yr}^{-1}$ ) is the same as that estimated by Raymond et al. (2013) (also  $32 \text{ Tg}$   
574  $\text{C yr}^{-1}$ ), downscaled over the same basin area, but smaller than the  $59.7 \text{ Tg C yr}^{-1}$  calculated by  
575 Lauerwald et al. (2015) and far smaller than that of Borges et al. (2015<sup>a</sup>),  $133\text{-}177 \text{ Tg C yr}^{-1}$  or  
576 Borges et al. (2019),  $251\pm 46 \text{ Tg C yr}^{-1}$ . The recent study of Borges et al. (2019) is based on by  
577 far and away the most extensive dataset of Congo basin  $p\text{CO}_2$  measurements to date and thus  
578 suggests that we substantially underestimate total riverine  $\text{CO}_2$  evasion. As previously  
579 discussed, we simulate the broad spatial and temporal variation in observed DOC and  $p\text{CO}_2$   
580 (2015<sup>a, b</sup>, Fig. 5, Table 3) relatively well. It is therefore somewhat surprising that our basin-  
581 wide estimate of riverine  $\text{CO}_2$  evasion is so different. Below we discuss some possible  
582 explanations for this discrepancy related to methodological differences and limitations.

583 One potential cause for the differences could be the river gas exchange velocity  $k$ . We applied  
584 a mean riverine gas exchange velocity  $k_{600}$  of  $3.5 \text{ m d}^{-1}$  which is similar to the  $2.9 \text{ m d}^{-1}$  used  
585 by Borges et al. (2015<sup>a</sup>) but substantially smaller than the mean of approximately  $8 \text{ m d}^{-1}$   
586 estimated across Strahler orders 1-10 in Borges et al. (2019) (taking the contributing water  
587 surface area of each Strahler order into account). A sensitivity analysis was performed in  
588 Lauerwald et al. (2017) which showed that in the physical approach of ORCHILEAK,  $\text{CO}_2$   
589 evasion is not very sensitive to the  $k$  value, unlike data-driven models. Namely, Lauerwald et

590 al (2017) showed that an increase or decrease of  $k_{600}$  for rivers and swamps (flooded forests)  
591 of 50% only led to 1% and -4% change in total CO<sub>2</sub> evasion, respectively. In ORCHILEAK,  $k$   
592 does have an important impact on  $p\text{CO}_2$ ; i.e. a lower  $k$  value will increase  $p\text{CO}_2$ , but this will  
593 also lead to a steeper water-air CO<sub>2</sub> gradient and so ultimately to approximately the same  $F\text{CO}_2$   
594 over time. In other words, over the scales covered in this research (the large catchment area  
595 and water residence times of the Congo),  $F\text{CO}_2$  is mainly controlled by the allochthonous  
596 inputs of carbon to the river network, because by far the largest fraction of these C inputs is  
597 leaving the system via CO<sub>2</sub> emission to the atmosphere (as opposed to being laterally  
598 transferred downstream). Therefore, we do not consider  $k$  to be a major source of the  
599 discrepancy. Additionally, our  $k_{600}$  value of 0.65 m d<sup>-1</sup> for forested floodplains (based on Richey  
600 et al., 2002) compares well to recent a study which directly measured  $k_{600}$  on two different  
601 flooded forest sites in the Amazon basin, observing a range of 0.24 to 1.2 m d<sup>-1</sup> (MacIntyre et  
602 al., 2019).

603 Another potential reason for our smaller riverine CO<sub>2</sub> evasion could be river surface area. We  
604 simulate a mean present day (1980-2010) total river surface area of 25,900 km<sup>2</sup>, compared to  
605 the value of 23,670 km<sup>2</sup> used in Borges et al (2019, supplementary information) and so  
606 similarly we think that this can be discounted as a major source of discrepancy. However, it  
607 should be noted that both estimates are high compared to the recent estimate of 17,903 km<sup>2</sup>  
608 based on analysis of Landsat images (Allen & Pavelsky, 2018).

609 The difference in our simulated riverine CO<sub>2</sub> evasion compared to the empirically derived  
610 estimate of Borges et al. (2019), could be caused by the lack of representation of aquatic plants  
611 in the ORCHILEAK model. Borges et al. (2019) used the stable isotope composition of  $\delta^{13}\text{C}$ -  
612 DIC to determine the origin of dissolved CO<sub>2</sub> in the Congo River system and found that the  
613 values were consistent with a DIC input from the degradation of organic matter, in particular  
614 from C<sub>4</sub> plants. Crucially, they further found that the  $\delta^{13}\text{C}$ -DIC values were unrelated to the

615 contribution of *terra-firme* C<sub>4</sub> plants, rather that they were more consistent with the degradation  
616 of aquatic C<sub>4</sub> plants, namely macrophytes. ORCHILEAK does not represent aquatic plants, and  
617 the wider LSM ORCHIDEE does not have an aquatic macrophyte PFT either (though root  
618 respiration of floodplain plants for the PFTs represented, is accounted for as a C source). This  
619 could at the very least partly explain our conservative estimate of river CO<sub>2</sub> evasion, given that  
620 tropical macrophytes have relatively high NPPs. Rates as high as 3,500 g C m<sup>-2</sup> yr<sup>-1</sup> have been  
621 measured on floodplains in the Amazon (Silva et al., 2009). While this value is higher than the  
622 values simulated in the Cuvette Centrale by ORCHILEAK (Figure 8), they are of the same  
623 order of magnitude and so this alone cannot fully explain the discrepancy compared to the  
624 results of Borges et al. (2019). In the Amazon basin it has been shown that wetlands export  
625 approximately half of their gross primary production (GPP) to the river network compared to  
626 upland (*terra-firme*) ecosystems which only export a few percent (Abril et al. 2013). More  
627 importantly, Abril et al. (2013) found that tropical aquatic macrophytes export 80% of their  
628 GPP compared to just 36% for flooded forest. Therefore, the lack of a bespoke macrophyte  
629 PFT is indeed likely to be one reason for the discrepancy between our results and those of  
630 Borges, but largely due to their particularly high export efficiency to the river-floodplain  
631 network as opposed to differences in NPP. While being a significant limitation, creating and  
632 incorporating a macrophyte PFT would be a substantial undertaking given that the authors are  
633 unaware of any published dataset which has systematically mapped their distribution and  
634 abundance. It is important to note that while ORCHILEAK does not include the export of C  
635 from aquatic macrophytes it also neglects their NPP. Moreover, most aquatic macrophytes  
636 described in the literature have short (<1 year) life-cycles (Mitchel & Rogers, 1985). As such,  
637 while this model limitation is likely one of the causes for our relatively low estimate of riverine  
638 CO<sub>2</sub> evasion, it will only have a limited net effect on our estimate of the overall annual C  
639 balance (NBP, NEP) of the Congo basin.

640 Finally, another cause for the difference in riverine CO<sub>2</sub> evasion could be that the resolution of  
641 ORCHILEAK (0.5 degree river network and 1° for C fluxes) is not sufficient to fully capture  
642 the dynamics of the smallest streams of the Congo Basin which have been shown to have the  
643 highest DOC and CO<sub>2</sub> concentrations (Borges et al., 2019). Indeed, ORCHILEAK typically  
644 does not simulate the highest observed *p*CO<sub>2</sub> measurements of the smallest tributaries (i.e. >  
645 16,000 ppm). This is partly because for the fast reservoir (headwaters) in ORCHILEAK we  
646 assume full *p*CO<sub>2</sub> equilibrium with the atmosphere over one full day, which prevents very high  
647 *p*CO<sub>2</sub> values from building in the water column.

648 Despite these limitations, it is important to note that in our simulations, the evasion flux from  
649 rivers only contributes 15% of total aquatic CO<sub>2</sub> evasion, and including the flux from  
650 wetlands/floodplains, we produce a total of 235 Tg C yr<sup>-1</sup>. Moreover, the majority of this  
651 evasion occurs in the Cuvette Centrale (Fig. 8) which suggests that while ORHILEAK fails to  
652 attribute a large portion of this flux to small rivers (owing to the coarse resolution of the river  
653 network) we nonetheless do capture the source of carbon. In other words, in ORCHILEAK the  
654 majority of this carbon evades directly from the floodplain and wetlands of the Cuvette  
655 Centrale as opposed to the small rivers.

656 Our simulated export of C to the coast of 15 (15.3) Tg C yr<sup>-1</sup> is virtually identical to the  
657 TOC+DIC export estimated by Borges et al. (2015<sup>a</sup>) of 15.5 Tg C yr<sup>-1</sup>, which is consistent with  
658 the fact that we simulate a similar spatial variation of DOC concentrations (Fig. 8 and Fig. 1  
659 for locations). It is also relatively similar to the 19 Tg C yr<sup>-1</sup> (DOC + DIC) estimated by  
660 Valentini et al. (2014) in their synthesis of the African carbon budget. Valentini et al. (2014)  
661 used the largely empirical based Global Nutrient Export from WaterSheds (NEWS) model  
662 framework and they point out that Africa was underrepresented in the training data used to  
663 develop the regression relationships which underpin the model, and thus this could explain the  
664 small disagreement.

665 Of the total 15 Tg C yr<sup>-1</sup> exported to the coast, we simulate a 2.4 Tg C yr<sup>-1</sup> component of  
666 dissolved CO<sub>2</sub>, which is relatively similar to the empirically derived estimate of the total DIC  
667 export of 3.3 Tg C yr<sup>-1</sup> calculated in Wang et al. (2013). According to Wang et al., dissolved  
668 CO<sub>2</sub> accounts for the majority (1.9 Tg C yr<sup>-1</sup>) with the rest being the weathering derived flux  
669 of HCO<sub>3</sub><sup>-</sup>. Thus, the discrepancy between the two estimates is likely to be largely caused by  
670 our lack of accounting for the weathering derived flux (HCO<sub>3</sub><sup>-</sup>) which they estimate at 1.4 Tg  
671 C yr<sup>-1</sup>. In summary, despite this model limitation the results of Wang et al. (2013) suggest that  
672 we still capture the majority of the DIC flux.

673

#### 674 **4.2 Trends in terrestrial and aquatic carbon fluxes**

675 There is relatively sparse observed data available on the long-term trends of terrestrial C fluxes  
676 in the Congo. Yin et al. (2017) used MODIS data to estimate NPP between 2001 and 2013  
677 across central Africa. They found that NPP increased on average by 10 g C m<sup>-2</sup> per year, while  
678 we simulate an average annual increase of 4 g C m<sup>-2</sup> yr<sup>-1</sup> over the same period across the Congo  
679 Basin. The two values are not directly comparable as they do not cover precisely the same  
680 geographic area but it is encouraging that our simulations exhibit a similar trend to remote  
681 sensing data. As previously noted, MODIS derived estimates of NPP do not fully include the  
682 effect of CO<sub>2</sub> fertilization (de Kauwe et al., 2016) whereas ORCHILEAK does. Thus, the  
683 MODIS NPP product may underestimate the increasing trend in NPP, which would bring our  
684 modeled trend further away from this dataset. On the other hand, forest degradation effects and  
685 recent droughts have been associated with a decrease of greenness (Zhou et al., 2014) and  
686 above ground biomass loss (Qie et al., 2019) in tropical forests.

687 Up to a point, our results also concur with estimates based on the upscaling of biomass  
688 observations (Lewis et al., 2009; Hubau et al., 2019). Lewis et al. (2009) up-scaled forest plot

689 measurements to calculate that intact tropical African forests represented a net uptake of  
690 approximately 300 Tg C yr<sup>-1</sup> between 1968 and 2007 and this is consistent with our NEP  
691 estimate of 275 Tg C yr<sup>-1</sup> over the same period. However, more recently an analysis based on  
692 an extension of the same dataset found that the above ground C sink in tropical Africa was  
693 relatively stable from 1985 to 2015 (Hubau et al., 2020).

694 A major source of the uncertainty associated with future projections of NPP and NEP comes  
695 from our limited understanding and representation of the CO<sub>2</sub> fertilization effect. Recent  
696 analysis of data from some of the longest-running Free-Air CO<sub>2</sub> Enrichment (FACE) sites,  
697 consisting of early-successional temperate ecosystems, found a 29.1 ± 11.7% stimulation of  
698 biomass over a decade (Walker et al., 2019). A meta-analysis (Liu et al., 2019) of seven  
699 temperate FACE experiments combined with process-based modelling also found substantial  
700 sensitivity (0.64 ± 0.28 PgC yr<sup>-1</sup> per hundred ppm) of biomass accumulation to atmospheric  
701 CO<sub>2</sub> increase, and the same study showed that ORCHIDEE model simulations were largely  
702 consistent with the experiments. However, other FACE experiments on mature temperate  
703 forests (Körner et al., 2005), as well as eucalyptus forests bring into question whether the  
704 fertilization effects observed in temperate FACE experiments can be extrapolated to other  
705 ecosystems. For example, the Swiss FACE study, a deciduous mature forest, found no  
706 significant biomass increase with enhanced CO<sub>2</sub> (Körner et al., 2005), while a FACE  
707 experiment on a mature eucalyptus forest in Australia found that while CO<sub>2</sub> stimulated an  
708 increase in C uptake through GPP, this did not carry to the ecosystem level, largely as a result  
709 of a concurrent increase in soil respiration (Jiang et al., 2020). Unfortunately, no results are yet  
710 available from any tropical FACE experiments, though the Amazon FACE experiment is  
711 underway and the eventual results will be crucial in developing our understanding of the CO<sub>2</sub>  
712 fertilization effect beyond the temperate zone.

713 With these limitations in our understanding of tropical forest ecosystems in mind, over the  
714 entire simulation period (1861-2099) we estimate that aquatic CO<sub>2</sub> evasion will increase by  
715 79% and the export of C to the coast by 67%. While, there are no long-term observations of  
716 aquatic CO<sub>2</sub> evasion in the Congo, a recent paper examined trends in observed DOC fluxes in  
717 the Congo at Brazzaville/Kinshasa over the last 30 years (Moukandi N’kaya et al. 2020). They  
718 found a 45% increase in the annual flux of DOC from 11.1 Tg C yr<sup>-1</sup> (mean from 1987-1993)  
719 to 16.1 Tg C yr<sup>-1</sup> (mean from 2006-2017). Comparing the same two periods, we find a smaller  
720 increase of 15% from 12.3 Tg C yr<sup>-1</sup> to 14.2 Tg C yr<sup>-1</sup>. While our increase is substantially  
721 smaller, these observations are still over relatively short time scales and thus interannual  
722 variations could have considerable influence over the means of the two periods. Irrespectively  
723 it is encouraging that observations concur with the overall simulated increasing trend. Perhaps  
724 most interesting is that Moukandi N’kaya et al. (2020) attribute this increase to hydrological  
725 changes and specifically an increase in flood events in the central basin (including the Cuvette  
726 Centrale). Over this period, we too attribute the increase in carbon fluxes to the coast in part to  
727 climate change (Fig. 11 d) and over the full simulation period, the largest increase in DOC and  
728 CO<sub>2</sub> leaching into the aquatic system occurs within the Cuvette Centrale (Fig. A1).

729 Comparing our results to models of other basins, our simulated increases in outgassing (79%)  
730 and the export of C to the coast (67%). are considerably greater than the 23% and 27% rises  
731 predicted for the Amazon basin (Lauerwald et al., 2020), over the same period and under the  
732 same scenario. This is largely due to the fact climate change is predicted to have a substantial  
733 negative impact on the aquatic C fluxes in the Amazon, something that we do not find for the  
734 Congo where rainfall is projected to substantially increase over the 21<sup>st</sup> century (RCP 6.0). In  
735 the Amazon, Lauerwald et al. (2020) show that while there are decadal fluctuations in  
736 precipitation and discharge, total values across the basin remain unchanged in 2099 compared  
737 to 1861. However, changes in the spatial distribution of precipitation mean that the total water

738 surface area actually decreases in the Amazon. Indeed, while we find an increase in the ratio  
739 of C exports to the LOAC/NPP from 3 to 5%, Lauerwald et al. (2020) find a comparative  
740 decrease.

741 Our simulated increase in DOC export to the coast up to the present day is smaller than findings  
742 recently published for the Mississippi River using the Dynamic Land Ecosystem Model  
743 (DLEM, Ren et al., 2016). In addition, the Mississippi study identified LUC including land  
744 management practices (e.g. irrigation and fertilization), followed by change in atmospheric  
745 CO<sub>2</sub>, as the biggest factors in the 40% increase in DOC export to the Gulf of Mexico (Ren et  
746 al., 2016). Another recent study (Tian et al., 2015), found an increase in DIC export from  
747 eastern North America to the Atlantic Ocean from 1901-2008 but no significant trend in DOC.  
748 They demonstrated that climate change and increasing atmospheric CO<sub>2</sub> had a significant  
749 positive effect on long-term C export while land-use change had a substantial negative impact.

### 750 **4.3 Limitations and further model developments**

751 It is important to note that we can have greater confidence in the historic trend (until present-  
752 day), as the future changes are more reliant on the skill of Earth System model predictions and  
753 of course on the accuracy of the RCP 6.0 scenario. As discussed above, our understanding and  
754 representation of CO<sub>2</sub> fertilization, especially in the tropics, is a major limitation. Moreover,  
755 the majority of land surface models, ORCHILEAK included in its current iteration, do not  
756 represent the effect of nutrient limitation on plant growth meaning that estimates of land C  
757 uptake may be too large (Goll et al., 2017). There are also considerable uncertainties associated  
758 with future climate projections in the Congo basin (Haensler et al., 2013). Nutrient limitation  
759 on growth and a better representation of effect of enhanced CO<sub>2</sub>, particularly with regards to  
760 soil respiration (Jiang et al., 2020) and tree mortality (Hubau et al., 2020), are two crucial  
761 aspects which need to be further developed.



762 Additionally, we do not account for methane fluxes from Congo wetlands, estimated at 1.6 to  
763 3.2 Tg (CH<sub>4</sub>) per year (Tathy et al., 1992), and instead assume that all C is evaded in the form  
764 of CO<sub>2</sub>. Another limitation is the lack of accounting for bespoke peatland dynamics in the  
765 ORCHILEAK model. ORCHILEAK is able to represent the general reduction in C  
766 decomposition in water-logged soils and indeed Hastie et al. (2019) demonstrated that  
767 increasing the maximum floodplain extent in the Amazon Basin led to an increase in NEP  
768 despite fueling aquatic CO<sub>2</sub> evasion because of the effect of reducing soil heterotrophic  
769 respiration. Furthermore, ORCHILEAK uses a “poor soils” mask forcing file (Fig. 2 j) based  
770 on the Harmonized World Soil Database (FAO/IIASA/ISRIC/ISS-CAS/JRC, 2009), which  
771 prescribes reduced decomposition rates in low nutrient and pH soils (e.g. Podzols and  
772 Arenosols). The effect of the “poor soils” forcing can clearly be seen in the spatial distribution  
773 of the soil C stock in Fig. A3, where the highest C storage coincides with the highest proportion  
774 of poor soils. Interestingly, this does not include the Cuvette Centrale wetlands (Fig. 1), an area  
775 which was recently identified as containing the world’s largest intact tropical peatland and a  
776 stock of around 30 Pg C (Dargie et al., 2017). One potential improvement that could be made  
777 to ORCHILEAK would be the development of a new tailored “poor soils” forcing file for the  
778 Congo Basin which explicitly includes Histosols, perhaps informed by the Soil Grids database  
779 (Hengl et al., 2014), to better represent the Cuvette Centrale. This could in turn, be validated  
780 and/or calibrated against the observations of Dargie et al. (2017). A more long-term aim could  
781 be the integration/ coupling of the ORCHIDEE-PEAT module with ORCHILEAK.  
782 ORCHIDEE-PEAT (Qiu et al., 2019) represents peat as an independent sub-grid hydrological  
783 soil unit in which peatland soils are characterized by peat-specific hydrological properties and  
784 multi-layered transport of C and water. Thus far, it has only been applied to northern peatlands,  
785 and calibrating it to tropical peatlands, along with integrating it within ORCHILEAK would  
786 require considerable further model development, but would certainly be a valuable longer-term

787 aspiration. This could also be applied across the tropical region and would allow us to  
788 comprehensively explore the implications of climate change and land-use change for tropical  
789 peatlands. In addition, ORCHILEAK does not simulate the erosion and subsequent burial of  
790 POC within river and floodplain sediments. Although it does not represent the lateral transfer  
791 of POC, it does incorporate the decomposition of inundated litter as an important source of  
792 DOC and dissolved CO<sub>2</sub> to the aquatic system; i.e. it is assumed that POC from submerged  
793 litter decomposes locally in ORCHILEAK. Moreover, previous studies have found that DOC  
794 as opposed to POC (Spencer et al., 2016; Bouillon et al., 2012) overwhelmingly dominates the  
795 total load of C in the Congo.

796 The representation of the rapid C loop of aquatic macrophytes should also be made a priority  
797 in terms of improving models such as ORCHILEAK, particularly in the tropics. As previously  
798 discussed, ORCHILEAK also fails to account for the weathering derived flux (HCO<sub>3</sub><sup>-</sup>). Finally,  
799 the issue of shifting cultivation demands further attention; at least for the present day a shifting  
800 cultivation forcing file could be developed based on remote sensing data (Tyukavina et al.,  
801 2018). For additional discussion of the limitations of ORCHILEAK, please also see Lauerwald  
802 et al. (2017) and Hastie et al. (2019).

## 803 **5. Conclusions**

804 For the present day, we show that aquatic C fluxes, and in particular CO<sub>2</sub> evasion, are important  
805 components of the Congo Basin C balance, larger than for example the combined fluxes from  
806 LUC and harvesting, with around 4% of terrestrial NPP being exported to the aquatic system  
807 each year. Our simulations show that these fluxes may have undergone considerable  
808 perturbation since 1861 to the present day, and that under RCP 6.0 this perturbation could  
809 continue; over the entire simulation period (1861-2099), we estimate that aquatic CO<sub>2</sub> evasion  
810 will increase by 79% and the export of C to the coast by 67%. We further find that the ratio of

811 C exports to the LOAC/NPP could increase from 3 to 5%, driven by both rising atmospheric  
812 CO<sub>2</sub> concentrations and climate change. This calls for long-term monitoring of C levels and  
813 fluxes in the rivers of the Congo basin, and further investigation of the potential impacts of  
814 such change. Our results also highlight the limitations of the current generation of land surface  
815 models and call for investment into further model development.

816

817 *Code availability.* A description of the general ORCHIDEE code can be found here:  
818 [http://forge.ipsl.jussieu.fr/orchidee/browser#tags/ORCHIDEE\\_1\\_9\\_6/ORCHIDEE](http://forge.ipsl.jussieu.fr/orchidee/browser#tags/ORCHIDEE_1_9_6/ORCHIDEE).

819 The main part of the ORCHIDEE code was written by Krinner et al. (2005). See d'Orgeval et  
820 al. (2008) for a general description of the river routing scheme. For the updated soil C module  
821 please see Camino Serrano (2015). For the source code of ORCHILEAK see Lauerwald et al.  
822 (2017)- <https://doi.org/10.5194/gmd-10-3821-2017-supplement>

823 For details on how to install ORCHIDEE and its various branches, please see the user guide:  
824 <http://forge.ipsl.jussieu.fr/orchidee/wiki/Documentation/UserGuide>

825 *Author contribution.* AH, RL, PR and PC all contributed to the conceptualization of the study.  
826 RL developed the model code, AH developed the novel forcing files for Congo, and AH  
827 performed the simulations. FP provided the GIEMS dataset for model validation. AH prepared  
828 the manuscript with contributions from all co-authors. RL and PR provided supervision and  
829 guidance to AH throughout the research. PR acquired the primary financial support that  
830 supported this research.

831 *Competing interests.* The authors declare that they have no conflict of interest.

832 *Financial support.* Financial support was received from the European Union's Horizon 2020  
833 research and innovation programme under the Marie Skłodowska- Curie grant agreement No.

834 643052 (C-CASCADES project). PR acknowledges funding from the European Union's  
835 Horizon 2020 research and innovation programme under Grant Agreement 776810 (project  
836 VERIFY). RL acknowledges funding from the ANR ISIPEDIA ERA4CS project and from the  
837 French state aid managed by the ANR under the  
838 'Investissements d'avenir' programme with the reference ANR-16-CONV-0003.

839

## 840 **References**

- 841 Abril, G., Martinez, J.-M., Artigas, L. F., Moreira-Turcq, P., Benedetti, M. F., Vidal, L., ...  
842 Roland, F. (2013). Amazon River carbon dioxide outgassing fuelled by wetlands. *Nature*,  
843 505, 395. Retrieved from <http://dx.doi.org/10.1038/nature12797>
- 844 Allen, G. H., & Pavelsky, T. M. (2018). Global extent of rivers and streams. *Science*,  
845 361(6402), 585–588. <https://doi.org/10.1126/science.aat0636>
- 846 Becker, M.; Papa, F.; Frappart, F.; Alsdorf, D.; Calmant, S.; Da Silva, J.S.; Prigent, C.;  
847 Seyler, F. Satellite-based estimates of surface water dynamics in the Congo River Basin. *Int.*  
848 *J. Appl. Earth Obs. Geoinf.* 2018, 196–209
- 849 Borges, A. V., Darchambeau, F., Teodoru, C. R., Marwick, T. R., Tamooch, F., Geeraert, N.,  
850 ... Bouillon, S. (2015)<sup>a</sup>. Globally significant greenhouse-gas emissions from African inland  
851 waters. *Nature Geoscience*, 8, 637. Retrieved from <https://doi.org/10.1038/ngeo2486>
- 852 Borges, A. V., Abril, G., Darchambeau, F., Teodoru, C. R., Deborde, J., Vidal, L. O., ...  
853 Bouillon, S. (2015)<sup>b</sup>. Divergent biophysical controls of aquatic CO<sub>2</sub> and CH<sub>4</sub> in the World's  
854 two largest rivers. *Scientific Reports*, 5, 15614. <https://doi.org/10.1038/srep15614>
- 855 Borges, A. V., Darchambeau, F., Lambert, T., Morana, C., Allen, G. H., Tambwe, E.,  
856 Toengaho Sembaito, A., Mambo, T., Nlandu Wabakhangazi, J., Descy, J.-P., Teodoru, C. R.,  
857 and Bouillon, S (2019).: Variations in dissolved greenhouse gases (CO<sub>2</sub>, CH<sub>4</sub>, N<sub>2</sub>O) in the  
858 Congo River network overwhelmingly driven by fluvial-wetland connectivity,  
859 *Biogeosciences*, 16, 3801–3834, <https://doi.org/10.5194/bg-16-3801-2019>.
- 860 Bouillon, S., Yambélé, A., Spencer, R. G. M., Gillikin, D. P., Hernes, P. J., Six, J., Merckx,  
861 R., and Borges, A. V.: Organic matter sources, fluxes and greenhouse gas exchange in the  
862 Oubangui River (Congo River basin), *Biogeosciences*, 9, 2045–2062,  
863 <https://doi.org/10.5194/bg-9-2045-2012>, 2012.
- 864 Bouillon, S., Yambélé, A., Gillikin, D. P., Teodoru, C., Darchambeau, F., Lambert, T., &  
865 Borges, A. V. (2014). Contrasting biogeochemical characteristics of the Oubangui River and  
866 tributaries (Congo River basin). *Scientific Reports*, 4, 5402. Retrieved from  
867 <https://doi.org/10.1038/srep05402>

868 Bowring, S. P. K., Lauerwald, R., Guenet, B., Zhu, D., Guimberteau, M., Tootchi, A.,  
869 Ducharne, A., and Ciais, P (2019)<sup>a</sup>: ORCHIDEE MICT-LEAK (r5459), a global model for  
870 the production, transport, and transformation of dissolved organic carbon from Arctic  
871 permafrost regions – Part 1: Rationale, model description, and simulation protocol, *Geosci.*  
872 *Model Dev.*, 12, 3503–3521, <https://doi.org/10.5194/gmd-12-3503-2019>, 2019.

873 Bowring, S. P. K., Lauerwald, R., Guenet, B., Zhu, D., Guimberteau, M., Regnier, P.,  
874 Tootchi, A., Ducharne, A., and Ciais, P (2019)<sup>b</sup>: ORCHIDEE MICT-LEAK (r5459), a global  
875 model for the production, transport and transformation of dissolved organic carbon from  
876 Arctic permafrost regions, Part 2: Model evaluation over the Lena River basin, *Geosci.*  
877 *Model Dev. Discuss.*, <https://doi.org/10.5194/gmd-2018-322>, in review, 2019.

878 Camino-Serrano, M., Guenet, B., Luysaert, S., Ciais, P., Bastrikov, V., De Vos, B., Gielen,  
879 B., Gleixner, G., Jornet-Puig, A., Kaiser, K., Kothawala, D., Lauerwald, R., Peñuelas, J.,  
880 Schrumpf, M., Vicca, S., Vuichard, N., Walmsley, D., and Janssens, I. A.: ORCHIDEE-  
881 SOM: modeling soil organic carbon (SOC) and dissolved organic carbon (DOC) dynamics  
882 along vertical soil profiles in Europe, *Geosci. Model Dev.*, 11, 937–957,  
883 <https://doi.org/10.5194/gmd-11-937-2018>, 2018

884 CBFP (Congo Basin Forest Partnership) (2009). The forests of the Congo Basin — State of  
885 the Forest 2008, Publications Office of the European  
886 Union, Luxembourg (2009), 10.2788/32259

887 Ciais, P., Piao, S.-L., Cadule, P., Friedlingstein, P., & Chédin, A. (2009). Variability and  
888 recent trends in the African terrestrial carbon balance. *Biogeosciences*, 6(9), 1935–1948.  
889 <https://doi.org/10.5194/bg-6-1935-2009>

890 Ciais, P., Yao, Y., Gasser, T., Baccini, A., Wang, Y., Lauerwald, R., ... Zhu, D. (2020).  
891 Empirical estimates of regional carbon budgets imply reduced global soil heterotrophic  
892 respiration. *National Science Review*. <https://doi.org/10.1093/nsr/nwaa145>

893 Cochonneau, G., Sondag, F., Guyot, J.-L., Geraldo, B., Filizola, N., Fraizy, P., Laraque, A.,  
894 Magat, P., Martinez, J.-M., Noriega, L., Oliveira, E., Ordonez, J., Pombosa, R., Seyler, F.,  
895 Sidgwick, J., and Vauchel, P.: The environmental observation and research project, ORE  
896 HYBAM, and the rivers of the Amazon basin, in: *Climate Variability and Change –*  
897 *Hydrological Impacts*, IAHS Publ. 308, edited by: Demuth, S., Gustard, A., Planos, E.,  
898 Scatena, F., and Servat, E., IAHS Press, UK, 44–50, 2006

899 Coynel, A., P. Seyler, H. Etcheber, M. Meybeck, and D. Orange (2005), Spatial and seasonal  
900 dynamics of total suspended sediment and organic carbon species in the Congo River, *Global*  
901 *Biogeochem. Cycles*, 19, GB4019, doi:[10.1029/2004GB002335](https://doi.org/10.1029/2004GB002335).

902 Creese, A., Washington, R., & Jones, R. (2019). Climate change in the Congo Basin:  
903 processes related to wetting in the December–February dry season. *Climate Dynamics*, 53(5),  
904 3583–3602. <https://doi.org/10.1007/s00382-019-04728-x>

905 Dargie, G. C., Lewis, S. L., Lawson, I. T., Mitchard, E. T. A., Page, S. E., Bocko, Y. E., &  
906 Ifo, S. A. (2017). Age, extent and carbon storage of the central Congo Basin peatland  
907 complex. *Nature*, 542, 86. Retrieved from <https://doi.org/10.1038/nature21048>

908 De Kauwe, M. G., Keenan, T. F., Medlyn, B. E., Prentice, I. C. and Terrer, C. (2016) Satellite  
909 based estimates underestimate the effect of CO<sub>2</sub> fertilisation on net primary  
910 productivity. *Nature Climate Change*, 6, 892-893

911 d'Orgeval, T., Polcher, J., & de Rosnay, P. (2008). Sensitivity of the West African  
912 hydrological cycle in ORCHIDEE to infiltration processes. *Hydrology and Earth System  
913 Sciences*, 12, 1387– 1401. <https://doi.org/10.5194/hess-12-1387-2008>

914 Drake, T. W., Raymond, P. A., & Spencer, R. G. M. (2018). Terrestrial carbon inputs to  
915 inland waters: A current synthesis of estimates and uncertainty. *Limnology and  
916 Oceanography Letters*, 3(3), 132–142. <http://doi.org/10.1002/lol2.10055>

917 Fan, L., Wigneron, J.-P., Ciais, P., Chave, J., Brandt, M., Fensholt, R., ... Peñuelas, J. (2019).  
918 Satellite-observed pantropical carbon dynamics. *Nature Plants*, 5(9), 944–951.  
919 <https://doi.org/10.1038/s41477-019-0478-9>

920 FAO/IIASA/ISRIC/ISS-CAS/JRC: Harmonized World Soil Database (version 1.1), FAO,  
921 Rome, 2009.

922 Fisher JB, Sikka M, Sitch S, Ciais P, Poulter B, Galbraith D, Lee J-E, Huntingford C, Viovy  
923 N, Zeng N, Ahlstrom A, Lomas MR, Levy PE, Frankenberg C, Saatchi S, Malhi Y. 2013  
924 African tropical rainforest net carbon dioxide fluxes in the twentieth century. *Phil Trans R  
925 Soc B* 368: 20120376. <http://dx.doi.org/10.1098/rstb.2012.0376>

926 Frieler, K., Lange, S., Piontek, F., Reyer, C. P. O., Schewe, J., Warszawski, L., ... Yamagata,  
927 Y. (2017). Assessing the impacts of 1.5 °C global warming – simulation protocol of the Inter-  
928 Sectoral Impact Model Intercomparison Project (ISIMIP2b). *Geosci. Model Dev.*, 10(12),  
929 4321–4345. <https://doi.org/10.5194/gmd-10-4321-2017>

930 Goll, D. S., Vuichard, N., Maignan, F., Jornet-Puig, A., Sardans, J., Violette, A., Peng, S.,  
931 Sun, Y., Kvakic, M., Guimberteau, M., Guenet, B., Zaehle, S., Penuelas, J., Janssens, I., and  
932 Ciais, P.: A representation of the phosphorus cycle for ORCHIDEE (revision 4520), *Geosci.  
933 Model Dev.*, 10, 3745-3770, <https://doi.org/10.5194/gmd-10-3745-2017>, 2017.

934 Guimberteau, M., Drapeau, G., Ronchail, J., Sultan, B., Polcher, J., Martinez, J.-M., Prigent,  
935 C., Guyot, J.-L., Cochonneau, G., Espinoza, J. C., Filizola, N., Fraizy, P., Lavado, W., De  
936 Oliveira, E., Pombosa, R., Noriega, L., and Vauchel, P.: Discharge simulation in the sub-  
937 basins of the Amazon using ORCHIDEE forced by new datasets, *Hydrol. Earth Syst. Sci.*, 16,  
938 911–935, <https://doi.org/10.5194/hess-16-911-2012>, 2012.

939 Gumbrecht, T., Roman-Cuesta, R. M., Verchot, L., Herold, M., Wittmann, F., Householder,  
940 E., Murdiyarso, D. (2017). An expert system model for mapping tropical wetlands and  
941 peatlands reveals South America as the largest contributor. *Global Change Biology*, 23(9),  
942 3581–3599. <https://doi.org/10.1111/gcb.13689>

943 Haensler, A., Saeed, F. and Jacob, D. (2013): Assessment of projected climate change signals  
944 over central Africa based on a multitude of global and regional climate projections. In:  
945 *Climate Change Scenarios for the Congo Basin*. [Haensler A., Jacob D., Kabat P., Ludwig F.  
946 (eds.)]. Climate Service Centre Report No. 11, Hamburg, Germany, ISSN: 2192-4058

947 Hastie, A., Lauerwald, R., Ciais, P., Regnier, P (2019). Aquatic carbon fluxes dampen the  
948 overall variation of net ecosystem productivity in the Amazon basin: An analysis of the

949 interannual variability in the boundless carbon cycle. *Global Change*  
950 *Biology*,; 25: 2094– 2111. <https://doi.org/10.1111/gcb.14620>

951 Hartmann, J., R. Lauerwald, and N. Moosdorf (2014), A brief overview of the GLObal RIver  
952 CHemistry Database, GLORICH, Procedia Earth Planet. Sci., **10**, 23–27.

953 Heinimann A, Mertz O, Frohking S, Egelund Christensen A, Hurni K, Sedano F, et al. (2017)  
954 A global view of shifting cultivation: Recent, current, and future extent. PLoS ONE 12(9):  
955 e0184479. <https://doi.org/10.1371/journal.pone.0184479>

956 Hengl, T., de Jesus, J. M., MacMillan, R. A., Batjes, N. H., Heuvelink, G. B. M., Ribeiro, E.,  
957 ... Ruiperez Gonzalez, M. (2014). SoilGrids1km-global soil information based on automated  
958 mapping. PLoS One, 9, e105992. <https://doi.org/10.1371/journal.pone.0105992>

959 Hubau, W.; Lewis, S.L.; Phillips, O.L.; Affum-Baffoe, K.; Beeckman, H.; Cuní-Sanchez, A.;  
960 Daniels, A.K.; Ewango, C.E.N.; Fauset, S.; Mukinzi, J.M.; et al. Asynchronous carbon sink  
961 saturation in African and Amazonian tropical forests. *Nature* 2020, 579, 80–87.

962 Hurtt, G. C., Chini, L. P., Frohking, S., Betts, R. A., Feddema, J., Fischer, G., ... Wang, Y. P.  
963 (2011). Harmonization of land-use scenarios for the period 1500--2100: 600 years of global  
964 gridded annual land-use transitions, wood harvest, and resulting secondary lands. *Climatic*  
965 *Change*, 109(1), 117. <https://doi.org/10.1007/s10584-011-0153-2>

966 Jiang, M., Medlyn, B.E., Drake, J.E. *et al.* The fate of carbon in a mature forest under carbon  
967 dioxide enrichment. *Nature* **580**, 227–231 (2020). <https://doi.org/10.1038/s41586-020-2128-9>

968 Kim, H. (2017). *Global Soil Wetness Project Phase 3 Atmospheric Boundary Conditions*  
969 *(Experiment 1)* [Data set]. Data Integration and Analysis System (DIAS).  
970 <https://doi.org/10.20783/DIAS.501>

971 Korner C, Asshoff R, Bignucolo O (2005) Carbon flux and growth in mature deciduous forest  
972 trees exposed to elevated CO2. *Science*, 309, 1360–1362.

973 Lange., S (2017). "ISIMIP2b Bias-Correction Code," *Zenodo*, doi: [10.5281/zenodo.1069050](https://doi.org/10.5281/zenodo.1069050)

974 Laudon, H., and I. Buffam (2008), Impact of changing DOC concentrations on the potential  
975 distribution of acid sensitive biota in a boreal stream network, *Hydrol. Earth Syst.*  
976 *Sci.*, **12**(2), 425–435.

977 Lauerwald, R., Laruelle, G. G., Hartmann, J., Ciais, P., & Regnier, P. A. G. (2015). Spatial  
978 patterns in CO2 evasion from the global river network. *Global Biogeochemical Cycles*, 29(5),  
979 534–554. <https://doi.org/10.1002/2014GB004941>

980 Lauerwald, R., Regnier, P., Camino-Serrano, M., Guenet, B., Guimberteau, M., Ducharne,  
981 A., ... Ciais, P. (2017). ORCHILEAK (revision 3875): a new model branch to simulate  
982 carbon transfers along the terrestrial--aquatic continuum of the Amazon basin. *Geoscientific*  
983 *Model Development*, 10(10), 3821–3859. <https://doi.org/10.5194/gmd-10-3In821-2017>

984 Lauerwald, R., Regnier, P., Guenet, B., Friedlingstein, P; Ciais, P (2020): How simulations of  
985 the land carbon sink are biased by ignoring fluvial carbon transfers – A case study for the  
986 Amazon basin. *One Earth*, 10.1016/j.oneear.2020.07.009.



987 Lee, H., Beighley, R. E., Alsdorf, D., Jung, H. C., Shum, C. K., Duan, J., ... Andreadis, K.  
988 (2011). Characterization of terrestrial water dynamics in the Congo Basin using GRACE and  
989 satellite radar altimetry. *Remote Sensing of Environment*, 115(12), 3530–3538.  
990 <https://doi.org/https://doi.org/10.1016/j.rse.2011.08.015>

991 Lehner, B., & Döll, P. (2004). Development and validation of a global database of lakes,  
992 reservoirs and wetlands. *Journal of Hydrology*, 296(1–4), 1–22.  
993 <https://doi.org/https://doi.org/10.1016/j.jhydrol.2004.03.028>

994 Lewis, S. L., Lopez-Gonzalez, G., Sonké, B., Affum-Baffoe, K., Baker, T. R., Ojo, L. O., ...  
995 Wöll, H. (2009). Increasing carbon storage in intact African tropical forests. *Nature*, 457,  
996 1003. Retrieved from <https://doi.org/10.1038/nature07771>

997 Liu, Y., Piao, S., Gasser, T., Ciais, P., Yang, H., Wang, H., ... Wang, T. (2019). Field-  
998 experiment constraints on the enhancement of the terrestrial carbon sink by CO<sub>2</sub> fertilization.  
999 *Nature Geoscience*, 12(10), 809–814. <https://doi.org/10.1038/s41561-019-0436-1>

1000 MacIntyre, S., Amaral, J. H. F., Barbosa, P. M., Cortés, A., Forsberg, B. R., & Melack, J.  
1001 M. (2019). Turbulence and gas transfer velocities in sheltered flooded forests of the Amazon  
1002 Basin. *Geophysical Research Letters*, 46, 9628–9636. <https://doi.org/10.1029/2019GL083948>

1004 Masui, T., Matsumoto, K., Hijioka, Y., Kinoshita, T., Nozawa, T., Ishiwatari, S., Kato, E.,  
1005 Shukla, P.R., Yamagata, Y., Kainuma, M., 2011. A emission pathway to stabilize at 6 W/m<sup>2</sup>  
1006 of radiative forcing, *Climatic Change*, doi:10.1007/s10584-011-0150-5. Morgan, M.G.,  
1007 Adams, P., Keith, D.W., 2006. Elicitation of expert judgments of aerosol forcing. *Climatic*  
1008 *Change* 75, 195–214

1009 Melack, J.M., Hess, L.L., Gastil, M., Forsberg, B.R., Hamilton, S.K., Lima, I.B. and Novo,  
1010 E.M. (2004), Regionalization of methane emissions in the Amazon Basin with microwave  
1011 remote sensing. *Global Change Biology*, 10: 530-544. doi:[10.1111/j.1365-2486.2004.00763.x](https://doi.org/10.1111/j.1365-2486.2004.00763.x)

1012 Mitchell D.S., Rogers K.H. (1985) Seasonality/aseasonality of aquatic macrophytes in  
1013 Southern Hemisphere inland water. In: Davies B.R., Walmsley R.D. (eds) *Perspectives in*  
1014 *Southern Hemisphere Limnology*. Developments in Hydrobiology, vol 28. Springer,  
1015 Dordrecht

1016 Moukandi N’kaya et al. (2020) Temporal Variability of Sediments, Dissolved Solids and  
1017 Dissolved Organic Matter Fluxes in the Congo River at Brazzaville/Kinshasa, *Geosciences*  
1018 2020, 10, 341; doi:10.3390/geosciences10090341

1019 Nash, J. E., and J. V. Sutcliffe. 1970. River flow forecasting through conceptual models: Part  
1020 1. A discussion of principles. *J. Hydrology* 10(3): 282-290

1021 O’Loughlin, F., M. A. Trigg, G. J.-P. Schumann, and P. D. Bates (2013), Hydraulic  
1022 characterization of the middle reach of the Congo River, *Water Resour. Res.*, 49, 5059–5070,  
1023 doi:[10.1002/wrcr.20398](https://doi.org/10.1002/wrcr.20398).

1024 Pan, S., Dangal, S. R. S., Tao, B., Yang, J., & Tian, H. (2015). Recent patterns of terrestrial  
1025 net primary production in Africa influenced by multiple environmental changes. *Ecosystem*  
1026 *Health and Sustainability*, 1(5), 1–15. <https://doi.org/10.1890/EHS14-0027.1>



1027 Papa, F., Prigent, C., Aires, F., Jimenez, C., Rossow, W. B., and Matthews,  
1028 E. (2010). Interannual variability of surface water extent at the global scale, 1993–2004, *J.*  
1029 *Geophys. Res.*, 115, D12111, doi:[10.1029/2009JD012674](https://doi.org/10.1029/2009JD012674).

1030 Potapov, P. V, Turubanova, S. A., Hansen, M. C., Adusei, B., Broich, M., Altstatt, A., ...  
1031 Justice, C. O. (2012). Quantifying forest cover loss in Democratic Republic of the Congo,  
1032 2000–2010, with Landsat ETM+ data. *Remote Sensing of Environment*, 122, 106–116.  
1033 <https://doi.org/https://doi.org/10.1016/j.rse.2011.08.027>

1034 Potter, C., Klooster, S., & Genovese, V. (2012). Net primary production of terrestrial  
1035 ecosystems from 2000 to 2009. *Climatic Change*, 115(2), 365–378.  
1036 <https://doi.org/10.1007/s10584-012-0460-2>

1037 Prigent, C., Papa, F., Aires, F., Rossow, W. B., and Matthews, E.: Global inundation  
1038 dynamics inferred from multiple satellite observations, 1993–2000, *J. Geophys. Res.*, 112,  
1039 D12107, <https://doi.org/10.1029/2006jd007847>, 2007.

1040 Qie, L., Telford, E. M., Massam, M. R., Tangki, H., Nilus, R., Hector, A., & Ewers, R. M.  
1041 (2019). Drought cuts back regeneration in logged tropical forests. *Environmental Research*  
1042 *Letters*, 14(4), 45012. <https://doi.org/10.1088/1748-9326/ab0783>

1043 Qiu, C., Zhu, D., Ciais, P., Guenet, B., Peng, S., Krinner, G., Tootchi, A., Ducharne, A., and  
1044 Hastie, A.: Modelling northern peatland area and carbon dynamics since the Holocene with  
1045 the ORCHIDEE-PEAT land surface model (SVN r5488), *Geosci. Model Dev.*, 12, 2961–  
1046 2982, <https://doi.org/10.5194/gmd-12-2961-2019>, 2019.

1047 R Core Team. (2013). R: A language and environment for statistical computing. [Available at  
1048 <http://www.r-project.org/>]

1049 Raymond, P. A., Hartmann, J., Lauerwald, R., Sobek, S., McDonald, C., Hoover, M., . . .  
1050 Guth, P. (2013). Global carbon dioxide emissions from inland waters. *Nature*, 503(7476),  
1051 355–359. Retrieved from <https://doi.org/10.1038/nature12760>

1052 Regnier, P., Friedlingstein, P., Ciais, P., Mackenzie, F. T., Gruber, N., Janssens, I. A., ...  
1053 Thullner, M. (2013). Anthropogenic perturbation of the carbon fluxes from land to ocean.  
1054 *Nature Geosci.*, 6(8), 597–607. Retrieved from <http://dx.doi.org/10.1038/ngeo1830>

1055 Ren, W., H. Tian, W.-J. Cai, S. E. Lohrenz, C. S. Hopkinson, W.-J. Huang, J. Yang, B. Tao,  
1056 S. Pan, and R. He (2016), Century long increasing trend and variability of dissolved organic  
1057 carbon export from the Mississippi River basin driven by natural and anthropogenic forcing,  
1058 *Global Biogeochem. Cycles*, 30, 1288–1299, doi:10.1002/2016GB005395.

1059 Reynolds, C., Jackson, T. & Rawls, W. Estimating available water content by linking 424 the  
1060 FAO soil map of the world with global soil profile databases and pedo-transfer 425 functions.  
1061 *Am. Geophys. Union Fall Meet. EOS Trans. Spring Meet. Suppl.* 80, S132 426 (1999).

1062 Richey, J. E., Melack, J. M., Aufdenkampe, A. K., Ballester, V. M., & Hess, L. L. (2002).  
1063 Outgassing from Amazonian rivers and wetlands as a large tropical source of atmospheric  
1064 CO<sub>2</sub>. *Nature*, 416(6881), 617– 620. <https://doi.org/10.1038/416617a>

1065 Schimel D, Stephens BB, Fisher JB. 2015. Effect of increasing CO<sub>2</sub> on the terrestrial carbon  
1066 cycle. *Proceedings of the National Academy of Sciences, USA* 112: 436–441

1067 Sheffield, J., Goteti, G., & Wood, E. F. (2006). Development of a 50-Year High-Resolution  
1068 Global Dataset of Meteorological Forcings for Land Surface Modeling. *Journal of Climate*,  
1069 *19*(13), 3088–3111. <https://doi.org/10.1175/JCLI3790.1>

1070 Silva, T.S.F., Costa, M.P.F. & Melack, J.M. Annual net primary production of macrophytes  
1071 in the eastern Amazon floodplain. *Wetlands* (2009) *29*: 747. <https://doi.org/10.1672/08-107.1>

1072 Smith, W.K., Fox, A.M., MacBean, N., Moore, D.J.P. and Parazoo, N.C. (2020),  
1073 Constraining estimates of terrestrial carbon uptake: new opportunities using long-term  
1074 satellite observations and data assimilation. *New Phytol*, *225*: 105-112.  
1075 doi:[10.1111/nph.16055](https://doi.org/10.1111/nph.16055)

1076 Spencer, R. G. M., P. J. Hernes, B. Dinga, J. N. Wabakanghanzi, T. W. Drake, and J. Six  
1077 (2016), Origins, seasonality, and fluxes of organic matter in the Congo River, *Global*  
1078 *Biogeochem. Cycles*, *30*, 1105–1121, doi: 10.1002/2016GB005427.

1079 Sullivan, M. J. P., Talbot, J., Lewis, S. L., Phillips, O. L., Qie, L., Begne, S. K., ... Zemagho,  
1080 L. (2017). Diversity and carbon storage across the tropical forest biome. *Scientific Reports*, *7*,  
1081 39102. Retrieved from <https://doi.org/10.1038/srep39102>

1082 Tathy, J. P., B. Cros, R. A. Delmas, A. Marenco, J. Servant, and M. Labat (1992), Methane  
1083 emission from flooded forest in central Africa, *J. Geophys. Res.*, *97*(D6), 6159–6168,  
1084 doi:[10.1029/90JD02555](https://doi.org/10.1029/90JD02555).

1085 Tian, H., Q. Yang, R. G. Najjar, W. Ren, M. A. M. Friedrichs, C. S. Hopkinson, and S. Pan  
1086 (2015), Anthropogenic and climatic influences on carbon fluxes from eastern North America  
1087 to the Atlantic Ocean: A process-based modeling study, *J. Geophys. Res. Biogeosci.*, *120*,  
1088 752–772, doi:10.1002/2014JG002760.

1089 Tranvik, Lars J., Downing, John A., Cotner, James B., Loiselle, Steven A., Striegl, Robert  
1090 G., Ballatore, Thomas J., Dillon, Peter, Finlay, Kerri, Fortino, Kenneth, Knoll, Lesley  
1091 B., Kortelainen, Pirkko L., Kutser, Tiit, Larsen, Soren., Laurion, Isabelle, Leech, Dina  
1092 M., McCallister, S. Leigh, McKnight, Diane M., Melack, John M., Overholt, Erin, Porter,  
1093 Jason A., Prairie, Yves, Renwick, William H., Roland, Fabio, Sherman, Bradford  
1094 S., Schindler, David W., Sobek, Sebastian, Tremblay, Alain, Vanni, Michael J., Verschoor,  
1095 Antonie M., von Wachenfeldt, Eddie, Weyhenmeyer, Gesa A., (2009), Lakes and reservoirs  
1096 as regulators of carbon cycling and climate, *Limnology and Oceanography*, *54*, doi:  
1097 10.4319/lo.2009.54.6\_part\_2.2298.

1098 Tyukavina, A., Hansen, M. C., Potapov, P., Parker, D., Okpa, C., Stehman, S. V, ...  
1099 Turubanova, S. (2018). Congo Basin forest loss dominated by increasing smallholder  
1100 clearing. *Science Advances*, *4*(11). <https://doi.org/10.1126/sciadv.aat2993>

1101 Valentini, R., Arneth, A., Bombelli, A., Castaldi, S., Cazzolla Gatti, R., Chevallier, F., Ciais,  
1102 P., Grieco, E., Hartmann, J., Henry, M., Houghton, R. A., Jung, M., Kutsch, W. L., Malhi, Y.,  
1103 Mayorga, E., Merbold, L., Murray-Tortarolo, G., Papale, D., Peylin, P., Poulter, B.,  
1104 Raymond, P. A., Santini, M., Sitch, S., Vaglio Laurin, G., van der Werf, G. R., Williams, C.  
1105 A., and Scholes, R. J.: A full greenhouse gases budget of Africa: synthesis, uncertainties, and  
1106 vulnerabilities, *Biogeosciences*, *11*, 381–407, doi:10.5194/bg11-381-2014, 2014

1107 Verhegghen, A., Mayaux, P., de Wasseige, C., & Defourny, P. (2012). Mapping Congo Basin  
1108 vegetation types from 300 m and 1 km multi-sensor time series for carbon stocks and forest  
1109 areas estimation. *Biogeosciences*, 9(12), 5061–5079. <https://doi.org/10.5194/bg-9-5061-2012>

1110 Viovy, N.. (2018). *CRUNCEP Version 7 - Atmospheric Forcing Data for the Community*  
1111 *Land Model*. Research Data Archive at the National Center for Atmospheric Research,  
1112 Computational and Information Systems Laboratory. <http://rda.ucar.edu/datasets/ds314.3/>

1113 Walker AP, De Kauwe MG, Medlyn BE, Zaehle S, Iversen CM, Asao S, Guenet B, Harper  
1114 A, Hickler T, Hungate BA et al. 2019. Decadal biomass increment in early secondary  
1115 succession woody ecosystems is increased by CO2 enrichment. *Nature Communications* 10:  
1116 454

1117 Wang, Z. A., D. J. Bienvenu, P. J. Mann, K. A. Hoering, J. R. Poulsen, R. G. M. Spencer, and  
1118 R. M. Holmes (2013), Inorganic carbon speciation and fluxes in the Congo River, *Geophys.*  
1119 *Res. Lett.*, 40, doi:10.1002/grl.50160

1120 Weiss, L. C., Pötter, L., Steiger, A., Kruppert, S., Frost, U., & Tollrian, R. (2018). Rising  
1121 pCO<sub>2</sub> in Freshwater Ecosystems Has the Potential to Negatively Affect Predator-Induced  
1122 Defenses in *Daphnia*. *Current Biology*, 28(2), 327–332.e3.  
1123 <https://doi.org/https://doi.org/10.1016/j.cub.2017.12.022>

1124 Williams, C. A., Hanan, N. P., Neff, J. C., Scholes, R. J., Berry, J. A., Denning, A. S., and  
1125 Baker, D. A.: Africa and the global carbon cycle, *Carbon Balance and Management*, 2(3),  
1126 doi:10.1186/1750-0680-2-3, 2007.

1127 Yin, S., Li, X., & Wu, W. (2017). Comparative analysis of NPP changes in global tropical  
1128 forests from 2001 to 2013. *IOP Conference Series: Earth and Environmental Science*, 57(1),  
1129 12009. Retrieved from <http://stacks.iop.org/1755-1315/57/i=1/a=012009>

1130 Zhou, L., Tian, Y., Myneni, R. B., Ciais, P., Saatchi, S., Liu, Y. Y., ... Hwang, T. (2014).  
1131 Widespread decline of Congo rainforest greenness in the past decade. *Nature*, 509(7498), 86–  
1132 90. <https://doi.org/10.1038/nature13265>

1133 Zhuravleva, I., Turubanova, S., Potapov, P., Hansen, M., Tyukavina, A., Minnemeyer, S., ...  
1134 Thies, C. (2013). Satellite-based primary forest degradation assessment in the Democratic  
1135 Republic of the Congo, 2000-2010. *Environmental Research Letters*, 8(2), 24034.  
1136 <https://doi.org/10.1088/1748-9326/8/2/024034>

1137

1138

1139

1140

1141 *Appendix A*

1142

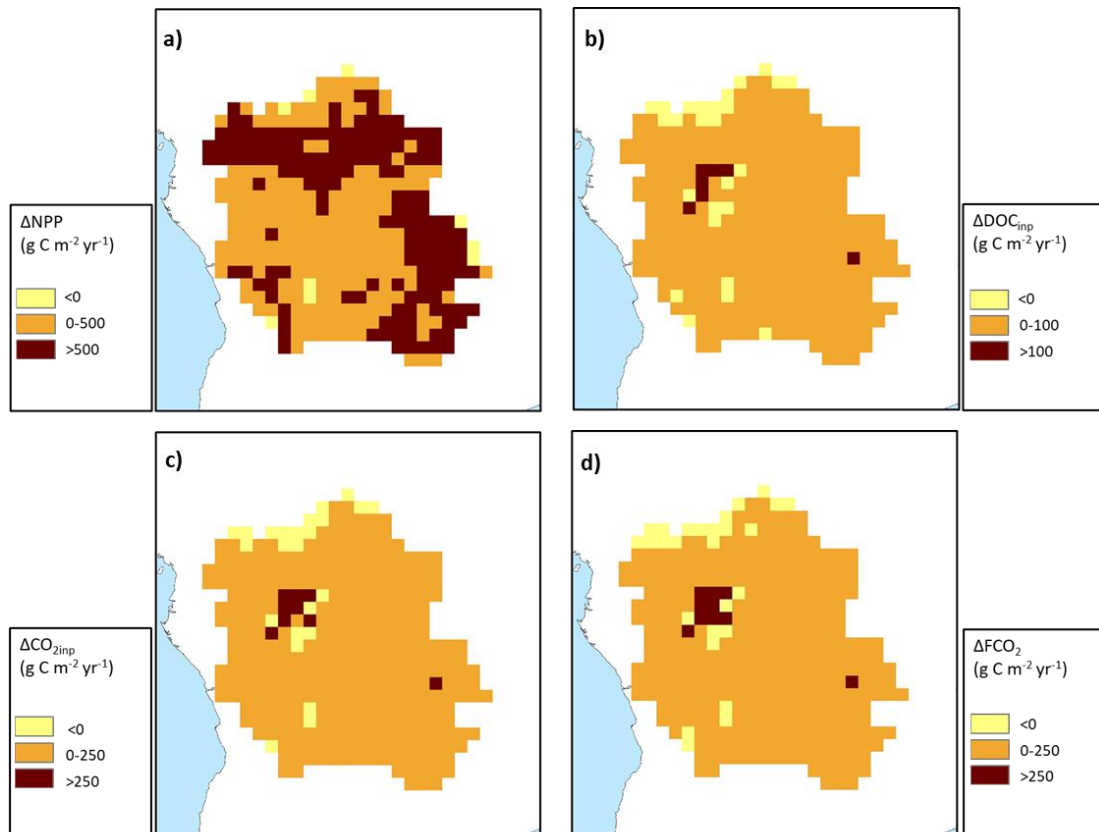
**Table A 1: Performance statistics for modelled versus observed seasonality of discharge on the Congo at Brazzaville**

Climate forcing	RSME	NSE	R <sup>2</sup>	Mean monthly discharge (m <sup>3</sup> s <sup>-1</sup> )
ISIMIP	29%	0.20	0.23	38,944
Princeton GPCC	40%	-0.25	0.20	49,784
GSWP3	46%	-4.13	0.04	24,880
CRUNCEP	65%	-15.94	0.01	16,394
Observed (HYBAM)				40,080

1143

**Table A 2: Pearson correlation coefficient (r) between detrended carbon fluxes and detrended climate variables**

	SHR	Aquatic CO <sub>2</sub> evasion	Lateral C	NEP	Rain	Temp.	MEI
NPP	-0.48	0.68	0.72	0.90	0.64	-0.57	-0.09
SHR		-0.41	-0.48	-0.71	-0.32	0.76	0.04
Aquatic CO <sub>2</sub> evasion			0.92	0.41	0.87	-0.30	-0.21
Lateral C				0.52	0.81	-0.38	-0.15
NEP					0.40	-0.74	-0.01
Rain						-0.31	-0.26
Temp.							0.03



1144

Figure A 1: Change ( $\Delta$ , 2099 minus 1861) in the spatial distribution of a) terrestrial NPP, b) DOC leaching into the aquatic system, c)  $\text{CO}_2$  leaching into the aquatic system and d) aquatic  $\text{CO}_2$  evasion. All at a resolution of  $1^\circ$

1145

1146

1147

1148

1149

1150

1151

1152

1153

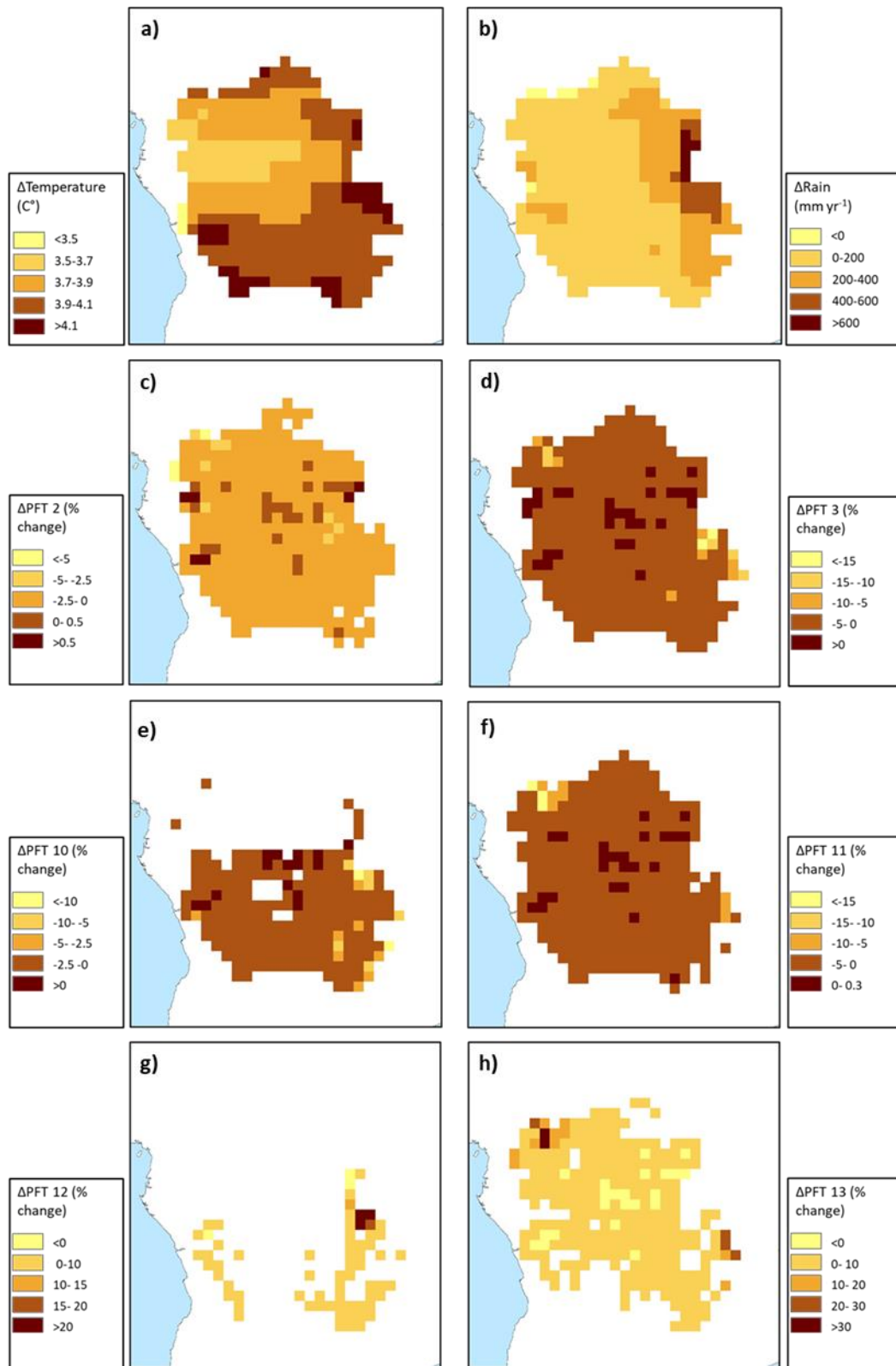


**Figure A 2:** Change ( $\Delta$ , 2099 minus 1861) in the spatial distribution of the principal climate and land-use drivers across the Congo Basin; a) mean annual temperature in °C, b) mean annual rainfall in mm yr<sup>-1</sup>, c)-h) mean annual maximum vegetated fraction for PFTs 2,3, 10,11,12 and 13. All at a resolution of 1°.

1155

1156

<b>Table A 3: Past (1861-1890), present-day (1981-2010) and future (2070-2099) mean values for important climate and land-use drivers across the Congo basin</b>								
Period	Temp.	Rain.	PFT2	PFT3	PFT10	PFT11	PFT12	PFT13
1861-1890	24.0	1451	0.263	0.375	0.154	0.254	0.015	0.014
1981-2010	25.2	1526	0.255	0.359	0.154	0.255	0.038	0.030
2070-2099	28.2	1654	0.258	0.362	0.147	0.245	0.039	0.037

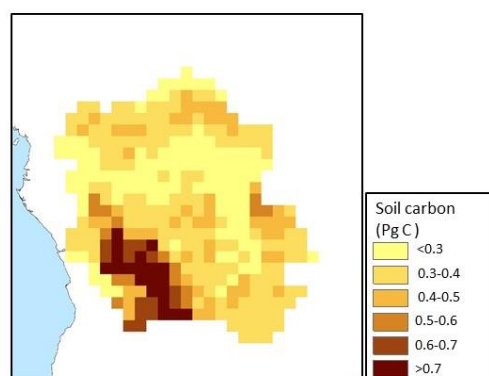


**Figure A 3: Spatial distribution of simulated total carbon stored in soils for the present day (1981-2020).**

1157

1158

1159